Åbo Akademi University

Dennis Kronlund

Chemical Engineering of Surface Coatings for Natural Stones

Laboratory of Physical Chemistry
Center for Functional Materials
Faculty of Science and Engineering

Chemical Engineering of Surface Coatings for Natural Stones

Dennis Kronlund

Laboratory of Physical Chemistry
Faculty of Science and Engineering
Åbo Akademi University
Åbo, Finland 2017

Supervised by:
Docent Jan-Henrik Smått
Laboratory of Physical Chemistry
Åbo Akademi University
Finland

Co-supervised by:
Professor Jouko Peltonen
Laboratory of Physical Chemistry
Åbo Akademi University
Finland

Reviewed by:
Professor Katarina Malaga
CBI Swedish Cement and Concrete Research Institute
Borås
Sweden

and

Associate Professor Marina Ruths
Department of Chemistry
College of Sciences
University of Massachusetts Lowell
USA

Opponent:
Professor Katarina Malaga
CBI Swedish Cement and Concrete Research Institute
Borås
Sweden

Printed version ISBN 978-952-12-3498-9
Digital version ISBN 978-952-12-3499-6
Painosalama Oy – Åbo, Finland 2017

"Long as I remember the rain been comin' down
Clouds of mystery pourin' confusion on the ground.
Good men through the ages tryin' to find the sun.
And I wonder still I wonder who'll stop the rain."

"Who'll Stop the Rain"

Creedence Clearwater Revival (John Fogerty)

Cosmo's factory, 1970

Abstract

Natural stones are materials widely used in today's architecture. White stones (such as marble) and speckled stones (such as granite) are regarded as suitable for decorative purposes and as construction materials. A major challenge with natural stones is that they degrade in nature through weathering effects, such as UV exposure, acid degradation as well as mechanical weathering through salt crystallization and ice formation inside the pores of the stones.

The overall objective of this work has been to develop different hydrophobization methods suitable for natural stones, with the goal of minimizing water contact with the stone substrates and consequently deterring weathering effects. Another goal was to develop testing methods for the evaluation of the protective effects of hydrophobic coatings on natural stones, when weathering was concerned.

In this study, a hydrophobic pore-lining coating for marble stones was produced via static and dynamic application methods. In the static systems using a total immersion method, a successful hydrophobization of marble stone products with a fluorosurfactant was verified by water contact angle and capillary absorption measurements before and after intentional UV degradation of the outmost modified layer. Optimization of treatment time and solution concentration led to marble stones that were fully protected from water absorption, even if the outermost surface was degraded by UV weathering. The functionalization method for hydrophobization of porous marble networks was further optimized by controlling the vesicle behavior of fluorosurfactants via tuning the solvent polarity and reaction temperature, leading to successful functionalization deep inside the porous network of the marble stones. This was confirmed by removing the outermost surface of the coated stones through mechanical grinding and measuring capillary absorption on the new surface, showing an increase in effective functionalization depth from μm to mm scale. The functionalization process was furthermore refined through the use of a spray coating method. The optimized spray coating conditions yielded an effective penetration of the fluorosurfactant into the pores of marble, ensuring a long-term protection against water uptake through pore wall functionalization. The final coating also displayed anti-graffiti properties, allowing for graffiti paint to repeatedly be easily washed away with a pressure washer 3-4 times. A new coating could be applied when the first coating lost its effectiveness.

Lastly, a durable surface coating based on polydimethylsiloxane for granite was studied to inhibit aging effects related to weathering of granite. The impact of several common weathering effects was evaluated by determining the mass loss, water contact angle, capillary water absorption and possible color alterations before and after the surface treatments. An important discovery was that the impact of the weathering tests on the pure granite was in most cases quite small, however, still noticeable and in some cases even considerable (especially concerning salt weathering). Furthermore, it was found out that sufficiently thick PDMS coatings displayed a superior stability in all the studied weathering tests compared to a reference coating, as the impact of weathering on the hydrophobic functionality of the PDMS-coated samples was minimal. Furthermore, due to the excellent water and salt blocking behavior, the PDMS-coated stones displayed an overall better stability against weathering compared to the untreated stones.

Svensk sammanfattning

Natursten såsom marmor och granit har länge använts som utgångsmaterial både inom konst och byggnadsteknik (till exempel för fasader). Ett stor problem är dock de nedbrytande vädereffekterna som natursten kan utsättas för, som till exempel solens UV-strålning och surt regn, men också mekaniska nedbrytningsmekanismer, såsom is-sprängning och saltkristallisering, vilka påverkar stenarnas porositet och mekaniska hållbarhet.

Målet med detta arbete har varit att utveckla ytmodifieringsmetoder för att göra naturstenar vattenavstötande, så att kontakten mellan stenarna och vatten minimeras och således minskar på vattenrelaterade vittringseffekter. Ett annat mål i detta arbete har varit att utveckla testmetoder som lämpar sig för undersökning av de vattenavstötande beläggningarnas funktionalitet i accelererad väderbeständighetstestning.

I avhandlingen behandlas en vattenavstötande ytbeläggning för marmorstenar som har framställts genom statiska och dynamiska modifieringsprocesser. I den statiska metoden gjordes modifieringen med marmorstenarna helt nedsänkta i en fluorosurfaktantlösning under bestämda förhållanden, varefter stenarna torkades i ugn samt ytbeläggningen undersöktes genom att mäta stenarnas vätningsbarhet samt kapillära absorption. Detta gjordes både direkt efter modifieringen samt efter att den yttersta ytbeläggningen hade brutits ned med hjälp av UV-ljus, för att undersöka ytbeläggningens modifieringsdjup.

Optimering av surfaktantkoncentrationen och behandlingstiden gav modifierade stenar som inte absorberade vatten över huvudtaget, även om den yttersta ytbeläggningen brutits ned av UV-ljus. Metoden utvecklades vidare genom att undersöka hur modifieringstemperaturen samt lösningsmedlets polaritet påverkade surfaktantaggregaten i lösningen. Detta resulterade i marmorstenar där ytbeläggningen hade trängt in flera millimeter i stenarna vilket förhindrade vattenabsorptionen helt även då två millimeter av den yttersta stenytan slipats bort. Studierna om hur micellaggregaten i lösningen påverkades av olika lösningsmedel påvisade att mera polära lösningsmedel förskjöt surfaktant-micelljämvikten mot fria surfaktanter, vilket resulterade i en bättre diffusion av surfaktantmolekylerna in i marmorns porer. Detta ledde i sin tur till en högre modifieringseringsgrad av marmorporytorna och en bättre vattenavstötande effekt.

Modifieringsprocessen utvecklades därefter till en mera praktisk spraybar appliceringsmetod. Den optimerade spraybara metoden kan producera marmorstenar med ytbelagda porer, vilket ger marmorstenarna ett långvarit skydd från nedbrytande vädereffekter. Den spraybara ytbeläggningen uppvisade också anti-graffitiegenskaper, vilket betyder att graffitifärg lätt kunde tvättas bort med en högtryckstvätt efter upprepade nedsmutsningar. När ytbeläggningens anti-graffitiegenskaper försämrades med upprepade tvättningar, kunde en ny beläggning appliceras för att förnya anti-graffitiegenskaperna.

Slutligen studerades en polydimetylsiloxan-beläggning för att förbättra granitstenars hållbarhet. Effekten av ett flertal vanligt förekommande nedbrytande fenomen undersöktes med accelererad väderbeständighetstestning och utvärderades genom mätningar av massförlust, kontaktvinklar, kapillär absorption och färgförändringar före och efter beläggning samt efter den simulerade nedbrytningen. Resultaten av dessa tester visade att de olika vittringsfenomenen bröt ned ren granit till olika grad och att den största effekten kunde ses då stenarna utsattes för saltsprängning, dvs. då en saltlösning bildar kristaller i porerna. Resultaten från de simulerade väderbeständighetstesterna påvisade även att en tillräckligt tjock polydimetylsiloxan-beläggning har en utomordentlig stabilitet i jämförelse med en referens-beläggning samt ren granit. Orsaken till detta var att de studerade väderfenomenen hade en minimal effekt på den hydrofoba polydimetylsiloxan-beläggningen till följd av den utmärkta motståndskraften mot vattenbaserade vittringseffekter.

List of publications

I. **Kronlund D.**, Bergbreiter A., Meierjohann A., Kronberg L., Lindén M., Grosso D., Smått J-H. **Hydrophobization of marble pore surfaces using a total immersion treatment method – Product selection and optimization of concentration and treatment time**. Progress in Organic Coatings 85 (2015) 159-167.

II. **Kronlund D.**, Bergbreiter A., Lindén M., Grosso D., Smått J-H. **Hydrophobization of marble pore surfaces using a total immersion treatment method – Influence of co-solvents and temperature on fluorosurfactant vesicle behavior**. Colloids and Surfaces A: Physicochemical Engineering Aspects 483 (2015) 104-111.

III. **Kronlund D.**, Lindén M., Smått J-H. **A spray coating method for making protective pore penetrating coatings on marble with water-repellent and anti-graffiti properties**. Progress in Organic Coatings 101 (2016) 359-366.

IV. **Kronlund D.**, Lindén M., Smått J-H. **A polymethylsiloxane coating to minimize weathering effects on granite**. Construction and Building Materials 124 (2016) 1051-1058.

Contributions of the author

The experimental work, analysis and writing of the first draft of the articles **I**, **II**, **III** and **IV** was carried out by the author with the following exceptions:

Paper **I**: M.Sc. Axel Meierjohann and Docent Leif Kronberg performed the mass spectrometry measurements and assisted with the results interpretation. M.Sc. Joel Songok performed the mercury intrusion porosimetry measurements, while Docent Jan-Henrik Smått performed the XRD measurements and assisted with the interpretation of the results.

Table of Contents

1. Introduction and outline

Natural stones are exposed to many degrading weathering phenomena occurring in nature, such as wind erosion, thermal variations, solar radiation and water processes, or combinations of several factors appearing simultaneously [1]. By considering the destructive effects of the most common weathering phenomena for porous calcareous stones (e.g. marble or sandstone); water vapor condensation, freezing, thawing, intraporous crystallization of salts, and acid rain dissolution, it becomes evident that it is a daunting task to inhibit the weathering phenomena completely. However, since water plays the dominant role in most of the above-mentioned weathering phenomena, eliminating water uptake into the porous stone is one of the key processes that necessitates investigation. Thus, the best way to protect such materials from degradation would be to prevent, or at least limit, the contact between the stone surface and water by making the stone and its pores hydrophobic [2].

Current research on the conservation of calcareous stone products is focused on developing effective surface coatings which at least partially reduce water absorption [2]. The use of hydrophobic polymers and polymer resins (e.g. fluorinated polymers and acrylic resins) is widespread due to their projected long-term stability [3-9]. Furthermore, a combination of sol-gel driven hydrophobic coatings with integrated nanoparticles have also been used in an effort to obtain biomimetic, super-hydrophobic stone surfaces [10-12] arising from a low surface energy and an enhanced surface roughness (i.e. the Lotus leaf effect [13-15]). An interesting stone protection approach that has garnered attention in recent years is the application of polydimethylsiloxane (PDMS) coatings and films [16-19], due to their elasticity, toughness and evenness. While the presented coatings in [16-19] displayed impressive hydrophobic functionality, no attempts have been done to study the durability of PDMS coatings on natural stones. So far, granite has not been widely studied in this field, due to its reputedly high stability against the degradation mechanisms commonly associated with other types of natural stones. Among the existing studies on granite, a hydrophobic functionalization of a biomimetic silica nanoparticle-alkoxysilane coating, which reduced the water uptake by ~20% can be mentioned [10]. Another interesting study, by Rosario et al, applies a novel consolidant along with commercial consolidants to granite, which improves the stone's resistance to salt crystallization weathering and slake durability [20].

It is remarkable that none of these treatments successfully inhibited water absorption completely in spite of exhibiting very high initial water contact angles when measured on the outer surface of the stone [3-6]. With time, both the polymer and sol-gel routes display significant water uptake [21] that could eventually damage the stone by any of the weathering phenomena described above. For polymeric compounds, this can be related to limited chemical bonding between the polymer and the stone, differences in the thermal expansion coefficients between the two components, as well as a low degree of pore surface modification [22]. A more persistent modification is expected if the hydrophobizing agent contains functional groups that can bind strongly to calcareous stone surfaces, e.g. phosphate, phosphonate or carboxylic groups [23-26]. However, as water can still, to some extent, be absorbed by the stone, the described degradation effects can continue even if they occur at a slower rate. It should also be noted that since $CaCO_3$ readily dissolves under slightly acidic conditions, even a small amount of water absorbed in the stone can lead to a loss of the outermost hydrophobized surface relatively quickly, which in turn will accelerate the degradation process. This implies that calcareous stones have to be functionalized deep inside the pore channels in order to provide a long-term stability.

In this thesis, a testing method suitable for assessing the penetration depth and functionality of a hydrophobization process targeted to porous natural stones is presented. Furthermore, a robust accelerated aging protocol is presented to assess the impact of destructive forces against natural stones, mainly for granite.

In Paper **I**, a total immersion functionalizing method was tuned for the hydrophobization of marble by controlling treatment time and solution concentration. Four fluorosurfactants as well as two fluorinated polymeric products were initially screened to identify which product resulted in the best water uptake protection and circumvented UV degradation. By further optimization of the functionalization protocol using the most promising compound, a fluorosurfactant, it was demonstrated that it is possible to improve the UV and chemical instabilities of common surface coatings, by not only modifying the outermost marble surface, but also the interior of the stones. It is shown that the treated marble stones are protected from water uptake even after the outer surface has intentionally been removed by strong UV irradiation, suggesting that the optimized coatings will be stable for several years of sunlight exposure.

In Paper **II**, the total immersion functionalizing method was tuned further by controlling the functionalization temperature and the solvent polarity. This is shown to control the vesicle behavior of the investigated fluorosurfactant, driving the vesicle-surfactant equilibrium towards free surfactants with increasing temperature and decreasing solvent polarity. The tuned conditions in the solution lead to favorable conditions in the Stokes-Einstein diffusion equation, improving the diffusion of the fluorosurfactant into the marble stones. The consequence of the improved diffusion was shown experimentally by removing the outermost surface of the coated stones through mechanical grinding and measuring capillary absorption on the new surface, demonstrating an increase in effective functionalization depth from μm to mm scale.

In Paper **III**, the fluorosurfactant functionalization was tuned for spray-coating application. The optimized application conditions showed an effective penetration depth of the hydrophobic properties down to at least 0.5 mm, ensuring a long-term protection against water uptake. Mechanistic studies of the functionalization process revealed that the solution mixtures containing ethylene glycol provide the best functionalization when a penetrating coating was preferred, due to the prolonged functionalization time as a consequence of the slow evaporation rate of the solvent combined with the beneficial shift in the surfactant-vesicle equilibrium towards free surfactants. The coatings also displayed anti-graffiti properties, allowing for graffiti paint to easily be washed away with a pressure washer repeatedly 3-4 times. For optimal re-usability of the anti-graffiti coatings, a new coating could be applied when the first coating loses its effectiveness.

In Paper **IV**, a surface coating for granite was studied, to demonstrate how the weathering effects granite was exposed to could be minimized by coating it with a sprayable polydimethylsiloxane functionalization. The impact of several common weathering effects (UV exposure, acid degradation, as well as mechanical weathering through salt crystallization and ice formation inside the pores) were evaluated. An important discovery was that the impact of the weathering tests on the pure granite is in most cases quite small, however still noticeable and in some cases even considerable (especially due to salt weathering). Furthermore, due to the excellent water and salt blocking behavior, the polydimethylsiloxane-coated stones displayed an overall better stability against weathering compared to untreated stones.

2. Background

2.1. Natural stones

Natural stone materials have always been in demand throughout the history of humankind, stretching back for at least 2.5 million years, when the earliest known Paleolithic stone tool technocomplex (i.e. the Olduwan) began [27]. The use of stone materials has always been widespread, with applications in flooring, cladding, facing, stairs, ornamental architecture, bathroom and kitchen countertops, funerary, furnishing, etc. The reason for this popularity is that natural stones have a very good durability and unique appearance, which is hard to imitate. Additionally, as natural stones are mined from the earth, it is very environmentally friendly compared to other construction materials.

Natural stones can be classified in three principal groups. The first, igneous rock (*latin* igneous=fire), is shaped through the solidification and cooling of magma or lava, which occurs through geothermal processes in the earth's crust. Examples of igneous rocks are granite, pumice and basalt. It has been estimated that about 65% of the earth's crust consist of igneous rocks.

The second group is sedimentary rocks, which form through sedimentation of fossils and rocks. Examples of sedimentary rocks are sandstone, limestone and gypsum. The sedimentary rocks account for about 8% of the earth's crust.

The third rock type is metamorphic rocks, which are formed through the restructuring of other rock types under temperatures and pressures that differ from those at which the original rock was formed. This metamorphosis is, essentially, a recrystallization process. Examples of metamorphic rocks are marble, gneiss and slate. The metamorphic rocks account for about 27% of the earth's crust [28].

2.1.1. Marble

Marble is a natural stone which is formed through metamorphism of sedimentary carbonate rocks such as limestone and dolomite rock (or even pre-existing marble). These rocks are recrystallized by high temperatures and pressure into a mineral containing larger crystals of interlocking mosaic of calcite and dolomite. The purity of the starting material in the metamorphism will play a large role in the appearance of the metamorphosed marble. Very pure limestone or dolomite

protoliths[1] will result in a pure, white marble, while mineral impurities such as clay, quartz and iron oxides will present itself as swirls, veins and even total green, black or brown coloring in the metamorphosed marble. Another important occurrence in the marble crystallization process is the micro-voids which form in marble during the metamorphosis and creates a low porosity stone. [29]

White marble has been used in art as a sculpting material since classical times. Properties that make marble such an excellent sculpting material include the low hardness of the material, making it easy to carve. Marble is also very homogeneous from a sculptor's viewpoint and has a low refractive index, allowing for light to penetrate deep into the material and giving it a unique luster. In architecture and building construction, marble is also used to highlight important buildings, such as the Finlandia Hall. Different applications of marble are shown in Figure 1.

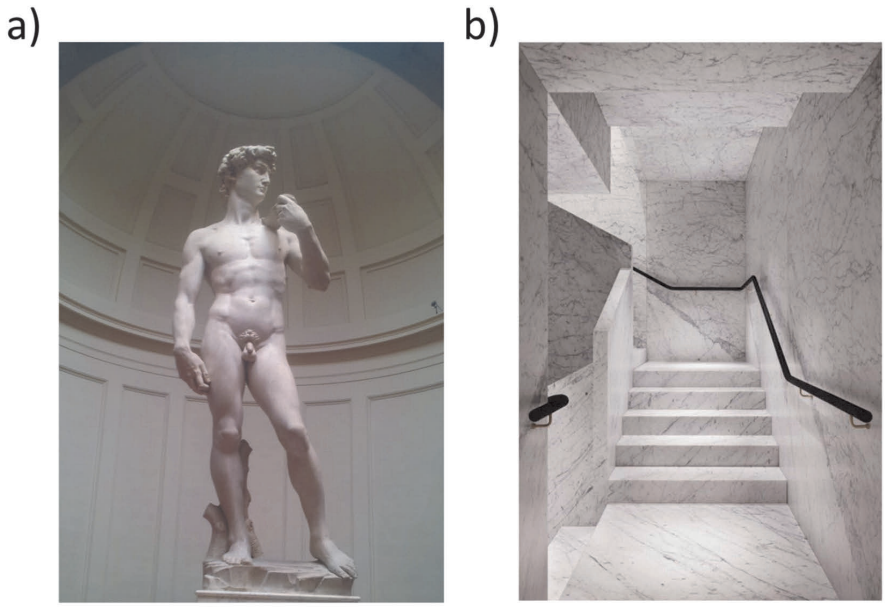

Figure 1. Different uses of marble, including a) the purely artistic David statue by Michelangelo, and b) utilized in interior design [30].

Marble is acquired by mining in quarries in different parts of the world, which have the conditions required for it to form, i.e. high pressure and sedimentary carbonate rocks. The regional variations in available protoliths for metamorphism account for that marble exists in several different crystal compositions with

[1] Protolith = the original rock, from which a given metamorphic rock is formed

different material properties depending on the conditions in which it has formed [31,32].

2.1.2. Granite

Granite is a common type of felsic[2] intrusive igneous rock that is granular and phaneritic[3] in texture. Granite is predominantly white, pink, or gray in color, depending on its mineralogy. The geological definition of granite is that it is a felsic rock with about 63 vol-% quartz. Granite have limited porosity, a high surface hardness and an inherent toughness, which is why it have been used throughout human history as a construction material [29].

Although both marble and granite are stone materials and are quarried from the earth, the stone types are very different from each other. The greatest difference lies in the lower porosity, hardness and durability of marble when compared to granite.

2.2. Challenges – aging effects on natural stones

Natural stones are exposed to several degrading weathering phenomena in nature, e.g. wind erosion, thermal variations, solar radiation and water phenomena are common effects. The degradation of natural stones is often not dependent on one distinct phenomenon, but a combination of several working together. The basic weathering phenomena investigated in this thesis will be covered in this section.

2.2.1. Physical phenomena

Physical weathering phenomena occur through mechanisms such as freeze-thaw processes, salt degradation, hygric[4], thermal and wet-dry cycling. As a consequence of these processes, the natural stone fragments along the preferred intra and intercrystalline microcracks, cleavage planes, joints, etc.

2.2.1.1. Frost weathering

Frost weathering is a form of physical degradation that can cause stone degradation through thermal variations in the freeze-thaw process during winter. When the temperature falls below 0 °C and water, which is absorbed in the pores of the stone, freezes and expands the formed ice applies pressure throughout the

[2] Felsic rock = Acidic igneous rock types that are relatively rich in elements that form feldspar (K-, Na- and Ca-$Al_xSi_xO_x$) and quartz (SiO_2)

[3] Phaneritic rock = rock type with crystals, which are discernible to the human eye

[4] Hygric = moisture-driven

porous stone, resulting in a degradation mechanism that is very severe for natural stones [33-35]. The degradation mechanism is schematically explained in Figure 2.

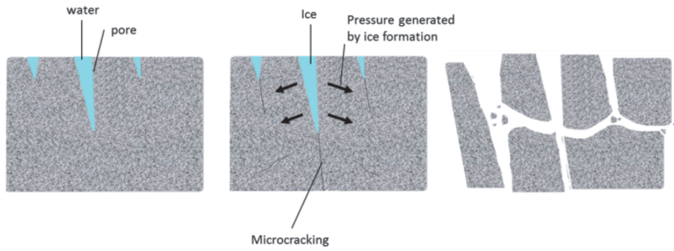

Figure 2. Degradation mechanisms caused be freezing and salt crystallization.

2.2.1.2. Salt crystallization

Salt crystallization in the pores of a natural stone is another form of physical degradation, where the formed crystals apply pressure on the porous network [20,36], causing stone degradation through the same mechanism as through ice formation (see Figure 2). This mechanism is particularly prevalent in coastal areas, where salt spray transport salts in the environment [37]. Another route of exposure is stone buildings and monuments submersed in water or exposed to waves from the salty sea. Common salts taking part in these degradation mechanisms are rock and sulfate salts [38,39].

2.2.2. Chemical phenomena

Chemical weathering phenomena are degradation processes that occur through the reactions that common substances, such as water, carbon dioxide and oxygen induce on the mineral constituents of natural stones. Chemical degradation is particularly damaging to natural stones that have complex systems of pores and grain boundaries, providing a relatively large surface area for the processes to occur on.

2.2.2.1. (Acid) rain degradation of stones

The penetration of rainwater into natural stones can also be a destructive force, e.g. as rainwater is slightly acidic, dissolution of calcareous stones is inevitable. The penetration of water into stones is linked to diffusion, capillary action, vapor pressure and surface tension, making it a difficult problem to solve [1]. Another problem that rain and seawater brings, besides dissolution, is the intraporous crystallization of salts transferred as ions with the water, which may damage the pore structure (see Chapter 2.2.1.1). Acid rain in itself often dissolves the outer crust of stones. The main responsible chemicals are nitrous oxides (NO_x) and

sulfuric oxides (SO_x). For instance the dissolution reaction of calcium carbonate when exposed to SO_2 is [40]:

$$CaCO_3(s) + SO_2(aq) + ½H_2O(l) \rightleftharpoons CaSO_3 \cdot ½H_2O(s) + CO_2(g). \quad (1)$$

The calcium sulfite hemi-hydrate ($CaSO_3 \cdot ½H_2O$) formed in the reaction is an unstable reaction product which is oxidized to gypsum ($CaSO_4 \cdot 2H_2O$) according to:

$$CaSO_3 \cdot ½H_2O(s) + ½O_2(g) + 2H_2O(l) \rightleftharpoons CaSO_4 \cdot 2H_2O(s) + ½H_2O(l). \quad (2)$$

Gypsum is then removed from the stone surface through erosion, and the stone is structurally damaged.

Although granite is a much more durable material than marble, it can also slowly degrade through hydrolysis, when the granite structure is disintegrated into granitic sand, a process that occurs through hydrolysis of the potassium feldspars (the binding network of granite) into clay minerals. The hydrolysis of granite proceeds via reactive H^+ ions which attempt to dissolve the mineral matrix, as for instance when K^+ ions in K-feldspar are replaced by H^+ ions according to [41-43]:

$$2\ KAlSi_3O_8 + H_2O + 2\ H^+ \rightleftharpoons Al_2Si_2O_5(OH)_4 + 2\ K^+ + 4\ SiO_2. \quad (3)$$

As K^+ and SiO_2 are water-soluble, these species are leached out from the system and kaolinite clay ($Al_2Si_2O_5(OH)_4$) remains. This weakens the structure of the material and causes it to break apart into smaller pieces.

A source of hydrogen ions in the atmosphere is the reaction carbon dioxide (CO_2) has with water, which forms carbonic acid (H_2CO_3). The carbonic acid is further dissociated into hydrogen ions and bicarbonate (HCO_3^-) according to [41-43]:

$$CO_2 + H_2O \rightleftharpoons H_2CO_3 \rightleftharpoons H^+ + HCO_3^-. \quad (4)$$

2.3. Challenges – graffiti

Graffiti is a large problem in our society as it sullies buildings and monuments. Keeping buildings free from graffiti defacing can be laborious and expensive, costing billions of euros annually, and it is particularly damaging to our cultural heritage [44,45], as seen in Figure 3.

Figure 3. Graffiti soiling the bell in Giotto's Campanile, Florence, Italy.

Graffiti can be applied in many different ways, with modern approaches ranging from stickers to marker pens and aerosol spray paints. Older school approaches include a hammer and a chisel, simple scratching and chalk or coal drawings.

Currently, there are two forms of graffiti paints that are dominating the market, i.e. water-based or oil-based paints. The water-based paints include emulsion (or latex) paint and (acrylic) waterborne pigment paints, which can be applied on hydrophilic substrates such as wood. On the other hand, oil-based paints like linseed oil paint are more suitable for oleophilic substrates. All graffiti paints consist of the same principal components; 1) a pigment, which gives the paint its color, 2) a binder, which holds the pigments together, and 3) a solvent, which makes the paint sprayable.

An interesting property of spray paints is that there is actually no chemical bond between the paint and the underlying surface. Paints adhere simply through physical van der Waals forces to the surface. The surface energy of a stone surface is therefore the deciding factor for the adherence of graffiti paints.

2.4. Methods of stone protection

2.4.1. Approaches

The longevity and usefulness of natural stones can be extended by applying a protective agent to the stone. These protective treatments can be applied with essentially three end results, as a) a pore-lining coating, b) a consolidating treatment and c) a surface film. These approaches are schematically drawn in Figure 4.

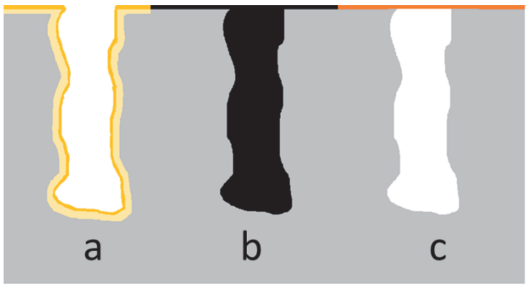

Figure 4. Different stone protection approaches, including a) a pore-lining coating, b) a consolidating coating and c) a surface film.

The pore-lining coating is a protective treatment that is performed with a molecularly small functionalization agent that is transported into the porous system of the stone via a carrier solution. Inside the pore system, the agent binds to the pore walls forming a thin layer throughout the stone. Chemicals that can be used as pore-lining coatings include silanes and surfactants. [46]

Consolidating stone treatments have been used since antiquity, when the Romans used olive oil to seal their stone materials. Olive oil consolidation treatments provided some protection by excluding water and other weathering agents from the porous network of the stone, although the stone was stained permanently by the oil. Modern stone sealers, also called penetrating sealers, include siliconates, fluoro-polymers and siloxanes. These sealers are employed as follows; a) the sealant solution containing a resin and mineral solvent or water is absorbed by the stone into the porous network, b) the mineral solvent or water evaporate and c) the resin remains, solidifies, and clogs the pores of the stone, anchoring the material in the stone. [47,48].

A surface film, sometimes referred to as a topical sealer, is a type of coating which solidifies on top of the stone surface, typically blocking water absorption, which also affects the water vapor permeability of the stone negatively. Maintaining the native water vapor permeability of a building material, such as natural stones, is very important. The reason for this is that condensation just under a protective coating is undesirable [12], as it will lead to stone decay as described in Chapter 2.1. Another drawback with surface films is that they are susceptible to peeling and scratching. Therefore, surface films require a routine of buffing, stripping and reapplication to maintain optimal functionality. On a molecular level, a surface film is formed when a large molecule cannot penetrate the pores of the substrate but instead dries and adheres to the surface. Common chemicals used for surface film formation include natural wax and polymers [5,12,49].

2.4.2. Methods of stone protection – mechanisms

Using the approaches mentioned above, different protective treatments can be performed on natural stones. A popular functionalization method used is hydrophobization, i.e. lowering the surface energy of stone surfaces with the end goal of minimizing water contact and consequently deterring water-related aging effects. The elimination of water has thus been a key aspect when protective coatings for natural stones have been developed [5,17,40,50]. Studied approaches include polymers [3-9], silicones [17,50-52] and sol-gel-derived hydrophobic coatings [13,53,54]. For marble, phosphates and carboxylates are preferred, due to the strong binding between the functional groups and calcium carbonate [24-26], while for granite silanes, silicates and siloxanes are particularly useful [10,20,55].

While consolidating functionalizations have drawbacks when the water vapor permeability is concerned, the positive effects these functionalizations can have should not be overlooked. By decreasing the porosity of the treated stone, weathering effects related to porosity, such as frost weathering, salt weathering and absorbed water effects [47,56] are minimized. Another benefit of consolidating coatings is the improved mechanical properties, such as increased abrasion resistance, surface hardness and compressive strength [48,57,58].

Stone functionalization is also used in the preparation of anti-graffiti coatings, such as sacrificial (often sugar-based) coatings [59,60]. These are used to create a surface film of a dissolvable coating that can be washed away with for instance warm water. A more permanent solution for keeping stone surfaces clean from graffiti is to use hydrophobic and oleophobic functional coatings [4], which minimize the adhesion of graffiti to the surface. This allows for the soiling color to be washed away with for example organic solvents or pressurized water [4,61].

A large weathering-related problem for the abovementioned stone coatings is caused by sunlight and particularly the UV portion of sunlight, which can cause damage to organic matter. The degradation mechanism occurs through the interaction of ultraviolet rays with chemical bonds in the organic structure, which forms free radicals that then react further with oxygen in the atmosphere. These radicals replace the existing organic chain with carbonyl groups and weaken the organic matter [62], which is particularly damaging to organic coating materials used in stone protection [63].

2.5. Interfacial properties

The interactions between water and the interfaces on natural stones are of great significance, when considering the different coatings discussed in this thesis. The complex surfaces studied here are heterogeneous, with varying porosities, leading to special considerations in the theory.

2.5.1. Adhesion and cohesion

It takes great force to pull many solids apart. A good example is diamonds, which are known for their high hardness. It is apparent that there must be a very strong attractive force between the carbon atoms in the diamond, which hold the material together. This force is cohesion, which is active in systems of similar materials. Adhesion, on the other hand, is active in systems of dissimilar materials, such as between a piece of adhesive tape and a piece of paper. Adhesive forces are active when surface atoms of two separate surfaces form ionic, covalent or hydrogen bonds. Forces between atoms or molecules, such as those in cohesion and adhesion, are effective only over very short distances (on the magnitude of molecular dimensions). Consequently, these forces are called short-range forces in contrast to forces such as gravitational attraction which is a long-range force.

2.5.2. Wetting and liquid spreading

Wetting, which occurs when a liquid comes into intimate contact with a solid surface, is dependent on the adhesive and cohesive forces interacting at the water-solid interface. The spreading coefficient at the liquid-solid interface, S_{LS}, is defined as [64]:

$$S_{LS} = W_A - W_C = \gamma_{SV} - \gamma_{LV} - \gamma_{SL}, \quad (5)$$

where W_A is the work of adhesion, W_C is the work of cohesion, γ_{SV} is the solid-vapor surface tension, γ_{LV} is the liquid-vapor surface tension and γ_{SL} is the solid-liquid surface tension. If S_{LS} is larger than zero, the liquid will completely wet the surface.

The spreading process is dependent on the surface properties of a solid. The adhesive interactions can for instance be manipulated by surface functionalization. When a water droplet comes into contact with a surface and when it does not wet the surface completely, it will spread until an equilibrium contact radius is reached. To model this, one has to account for the capillary, gravitational and viscous effects. The drop radius varies as a function of time according to [65]:

$$r(t) = \left[1 - exp\left(-\left(\frac{2\gamma_{LG}}{r_e^{12}} + \frac{\rho g}{9r_e^{10}}\right)\frac{24\lambda V^4(t+t_0)}{\pi^2\eta}\right)\right]^{\frac{1}{6}}, \quad (6)$$

However, when complete wetting occurs, the variation in drop radius during spreading is given as:

$$r(t) = \left[\left(\gamma_{LG}\frac{96\lambda V^4}{\pi^2\eta}(t+t_0)\right)^{\frac{1}{2}} + \left(\frac{\lambda(t+t_0)}{\eta}\right)^{\frac{2}{3}}\frac{24\rho g\lambda V^{\frac{3}{8}}}{7\cdot 96^{\frac{1}{3}}\pi^{\frac{4}{3}}\gamma_{LG}^{\frac{1}{3}}}\right]^{\frac{1}{6}}, \quad (7)$$

where γ_{LG} is the surface tension of the fluid, V is the drop volume, η is the viscosity of the fluid, ρ is the density of the fluid, g is the gravitational constant, λ is the shape factor, t_0 is the experimental delay time and r_e is the drop radius at equilibrium [65]. An example of the spreading process is given in Figure 5.

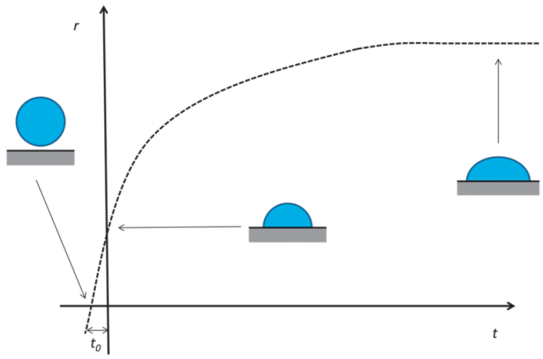

Figure 5. Example of the spreading process modelled by equation 6.

2.5.3. Flow and absorption in porous media

As natural stones are porous, the flow processes in porous media require special considerations as highlighted in Chapter 2.2. The elementary principles of fluid flow in porous media are highlighted here. The basic law governing flow in porous media is Darcy's law;

$$\dot{Q} = \frac{-\kappa A}{\mu}\frac{(p_b - p_a)}{L}. \quad (8)$$

For transient processes in which the flux varies from point to point, the differential form is used;

$$\dot{Q} = \frac{-\kappa A}{\mu}\left(\frac{dp}{dx}\right), \quad (9)$$

where $\dot{Q}$ is the volumetric flow rate, κ is the permeability of the porous medium, μ is the fluid viscosity, A is the cross-sectional area of the porous medium, $(p_b -$

p_a) is the pressure drop across the medium and L is the length of the sample [66]. Further developments of this law are needed to model pores of natural stones, because Darcy's law is excellent for modelling straight tube-like pores, while the pores of natural stones are more tortuous and have non-circular shapes. A modified Hagen-Poiseuille equation suggested by Cai et al. in [67] accounts for non-circular pore shapes and tortuosity according to:

$$q = \frac{\pi(\alpha r)^4 \Delta P}{8\mu L_a}, \tag{10}$$

where r is the pore radius and α is the dimensionless geometry correction factor, with α = 1 for circular capillaries, α = 1.094 for square capillaries and α = 1.186 for pores with equilateral triangular shapes. More data for α can be found in [68]. ΔP is the pressure loss, L_a is the actual length of the tortuous capillary pore and μ is dynamic viscosity.

As for water absorption through natural stone pores, which can be equated to thin capillaries, the traditional capillary rise model can be considered. If a capillary tube is immersed partially into a liquid, for instance water, the water will rise to a certain height inside the capillary. This height is positive for water (in a glass tube), while it is negative for mercury in the same glass tube, as mercury is a non-wetting liquid. If a very thin glass tube with the radius R is inserted into water, the water will climb the walls until the whole inside of the tube is covered by a thin layer of water, while a meniscus (the air-water interface in the tube) will rise to a certain height. This height, h, can be calculated considering the forces at work around the meniscus. At the meniscus, the physical force of interfacial tension can be defined as $2\pi R\gamma_{lv}$, i.e. the circumference of the pore multiplied by the surface tension. This force is opposing the gravitational pull on the water that has risen above the water surface level inside the cylinder. The gravitational force can be defined as $\pi R^2 h\rho g$, i.e. the volume ($\approx$ mass) of the water pillar multiplied by the gravitational acceleration. Using this information the height of the capillary rise can be calculated according to [64];

$$h = \frac{2\,\gamma_{lv}}{\rho g R}, \tag{11}$$

where R is the radius of the capillary and γ_{lv} is the interfacial tension between the liquid and the vapor, ρ is the liquid density and g is the gravitational acceleration

If the liquid in the cylinder is not completely wetting the whole cylinder, incomplete wetting is observed and a contact angle can be defined (see chapter

5.4 for more details on these). By consulting Figure 6, it becomes apparent that the interfacial tension will be reduced to $\cos(\theta)\gamma_{lv}$ and the capillary rise can be expressed as:

$$h = \frac{2\cos(\theta)\gamma_{lv}}{\rho g R}. \tag{12}$$

Equation 12 is a capillary rise equation that is valid for all systems, as for complete wetting and a contact angle of zero will result in a $\cos(\theta)$ of 1 (i.e. the equation is reduced to Equation 11). The result of equation 12 is illustrated in Figure 6.

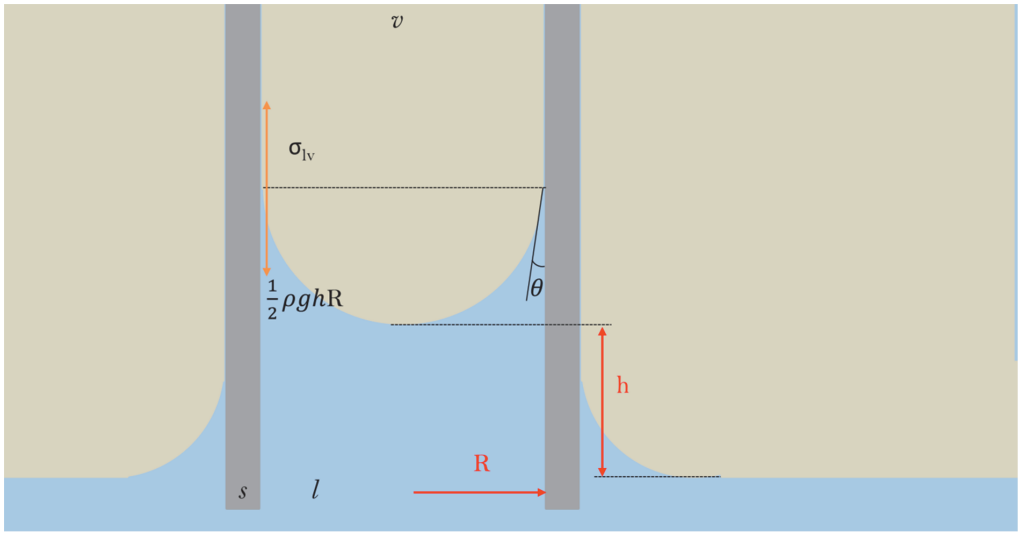

Figure 6. The capillary rise of a liquid in a smooth-walled capillary with the radius R.

Adhesive and cohesive forces can affect liquids inside the capillary in several ways. If the mutual attraction between water molecules in the system is very strong and the surface of the capillary wall is hydrophobic, i.e. has very weak interactions with the water molecules, the water molecules will strive to minimize contact with the wall and form a convex meniscus at the water-air interface. If, on the other hand, the surface of the wall is hydrophilic, the water molecules will be attracted to it and a concave meniscus will form, resulting in an increase in capillary rise, as illustrated in Figure 6.

While these models are excellent for modelling straight tube-like pores, the pores of natural stones are tortuous, interconnected and have variable cross-sectional areas, rendering them difficult to model exactly. However, the presented theory gives a basic understanding of the processes occurring in capillary absorption of water into natural stone pores and the importance of interfacial properties.

2.6. Surfactant chemistry

As surfactants were extensively studied in the marble functionalizations, the basics of surfactant chemistry are covered here. A surfactant is a molecule, which consist of a hydrophobic (water-repelling) part and a hydrophilic (water-attracting) part [64]. An example of a surfactant is depicted in Figure 7.

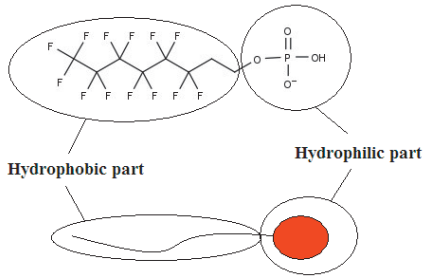

Figure 7. Schematic representation of a surfactant compared to the skeletal formula of a real surfactant, with a hydrophilic phosphate part and a hydrophobic fluorocarbon part.

Surfactants decrease the surface tension of liquids as their concentration increases in a solution. This decrease of the surface tension occurs linearly, depending on the surfactant concentration, c_s, as the molecules strive to arrange themselves in the most energetically favorable orientation, resulting in an accumulation of surfactants at the liquid-gas interface, e.g. a water surface in contact with air, as depicted in Figure 8 when $c_s <$ c.m.c. (critical micelle concentration).

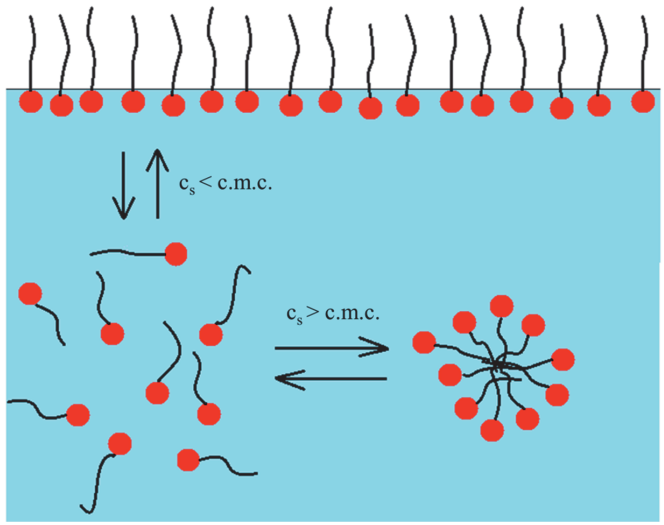

Figure 8. The mechanisms of surfactant accumulation at the air-liquid interface and micelle formation in the liquid phase. The red headgroup represents the hydrophilic group of the surfactant.

As the surfactant concentration reaches the c.m.c., the air-liquid interface becomes saturated with surfactants and the molecules start to self-assemble into aggregates, such as micelles and vesicles (depicted in Figure 8), when c_s > c.m.c.. The liquid-gas surface tension remains constant at concentrations above the c.m.c. Micelles, which are aggregates of surfactants, are formed to attain the most energetically favorable orientation of "hiding" the hydrophobic part of the surfactant (the black "tail" in Figure 8) when this occurs in water (as opposed to in oil, where the polar "head group " is "hidden" instead). Different types of micellar aggregate shapes are obtained depending on the surfactant form, as seen in Figure 9.

The Israelachvili model [69] can be used to account for variations in surfactant aggregation behavior (= association). The structural shape of the surfactants will influence the conformation of the micellar aggregates through the packing parameter *P*, defined as:

$$P = \frac{v}{a_0 l_c}, \tag{13}$$

where v is the volumetric space occupied by the hydrophobic tail group, a_0 is the optimal head group cross-sectional area and l_c the critical chain length. The different micellar aggregate structures that can be formed are summarized in Figure 9.

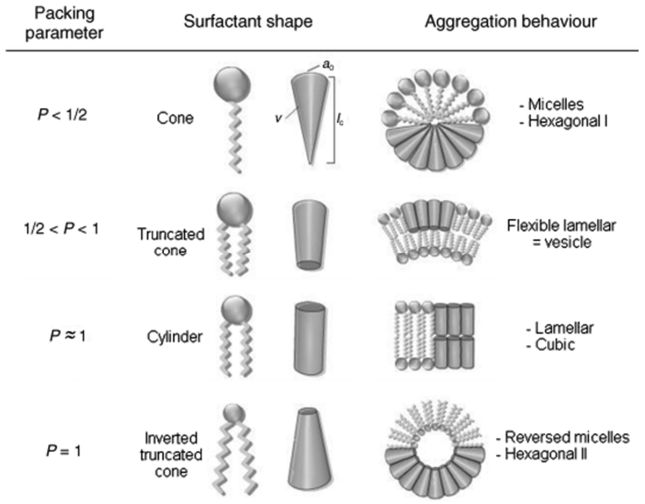

Figure 9. Different surfactant shapes and their resulting aggregation behavior, governed by the Israelachvili model as interpreted by Consola et al [70] [5].

[5] Note that Israelachvili defined the packing parameter of inverted truncated cone surfactants as P ≥ 1 [71].

Vesicles can occur in many different forms, as indicated in Figure 10. Some of the size ranges that could be mentioned are small unilamellar vesicles (SUVs, 20 to 50 nm in diameter), large unilamellar vesicles (LUVs, 100 nm to 1 μm in diameter) and giant unilamellar vesicles (GUVs, > 1 μm diameter). Furthermore, variations of these, such as the oligolamellar and multivesicular forms can occur, but they can still be classified in the groups of small, large and giant vesicles.

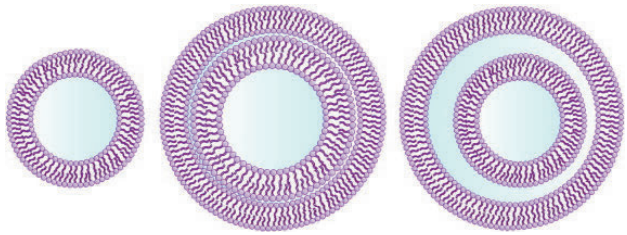

Figure 10. Schematics of unilamellar, oligolamellar and nested multivesicular vesicles [72].

An interesting feature of the surfactant-vesicle equilibrium, i.e. when c_s > c.m.c. in Figure 8, is that the equilibrium can be shifted by changing the polarity of the liquid or adding electrolytes to the solution. The equilibrium between free surfactants in the solution and the micellar aggregates consists of continuous demicellization and assembly [73-79]. The vesicle-surfactant equilibrium can shift towards free surfactants or other constitutions, such as from giant to small vesicle, which can be more suitable for diffusion into porous matrices, such as those found in natural stones. Furthermore, an increase in the solution temperature will change the polarity of the solvent and can thus also affect the vesicle stability [78-80].

3. Aims of the study

The goal of this thesis was to develop and evaluate a series of model systems suitable for stone protection. Recommendations were to be developed with the goal of a better coating and coating methods based on a materials science approach. This thesis focuses on case studies of granite and marble coatings to understand the benefits of a pore functionalization approach for marble. Another focus was to determine the most severe weathering effects that granite is exposed to.

The first model system to be studied was a pore-functionalized fluorosurfactant coating for marble stones. A broad study was carried out in order to evaluate different application parameters and determine how the composition of the fluorosurfactant solutions, in regard to their concentration and co-solvent composition, may affect the coating quality. The colloidal behavior and self-assembly of a fluorosurfactant was studied to improve the functionality of the surfactant coating with the end goal of a spray coating application approach for easy, low-cost coating. Additional functionality testing of the fluorosurfactant coating, as an environmentally friendly anti-graffiti coating, was also performed.

The second model system studied was a polymeric surface coating for granite stones. This system was studied through the formulation of test methods suitable for simulating aging effects to determine the impact of weathering on granite stones and the polymeric coatings.

The specific objectives of this thesis are:

- To evaluate the effects of time and surfactant concentration on marble surface functionalization when considering the effects on capillary absorption (**Paper I**)
- To evaluate the effects of temperature and solvent composition on the fluorosurfactant vesicle equilibrium and the consequences that the changes in this equilibrium can have on marble pore functionalization (**Paper II**)
- To investigate the sprayability of the fluorosurfactant formulation, with special consideration on the evaporation kinetics of the solutions and the beneficial properties of water- and oil-repellent surfaces as anti-graffiti coatings (**Paper III**)
- To investigate the impact of weathering effects on granite (**Paper IV**)
- To evaluate the durability of PDMS when used as a protective coating for granite (**Paper IV**)

4. Materials and methods

4.1. Materials

The characteristics of the stone substrates and functionalization agents used in this work are briefly described in this section.

4.1.1. Natural stones

Marble stones from Carrara, Italy, were used throughout the marble studies. Italian Carrara marble was used for its reputation of being a very chemically pure marble consisting almost entirely of calcite, $CaCO_3$, with some minor traces of dolomite, $CaMg(CO_3)_2$, which was confirmed through XRD (see Paper **I** for further details). The marble stones investigated had the dimensions of 2x2x1, 5x5x1 or 10x10x1 cm^3.

Granite from the Fujian province, China, was used throughout all the granite experiments. Stones with the dimensions of 5x5x1 cm^3 were used in all the tests, except for the frost weathering, where granite samples with the dimensions 2x2x1 cm^3 were used. The used granite stones consisted of silica, SiO_2, and the feldspars albite, $NaAlSi_3O_8$, anorthite, $CaAl_2Si_2O_8$, and sanidine, $KAlSi_3O_8$, which was confirmed through XRD (see Paper **IV** for further details).

The stones were washed in de-ionized water when received and dried in 60 °C for 1 week before any experiments were conducted. Note that it has been reported that marble stones may experience inter-granular decohesion under these circumstances [80].

4.1.2. Functionalizing agents

A commercially available fluorosurfactant, with the trade name Capstone FS-63 (Dupont), was used for the marble functionalizations. The structure of the fluorosurfactant in the commercial Capstone FS-63 mixture is depicted in Figure 11, along with the known structure of PDMS.

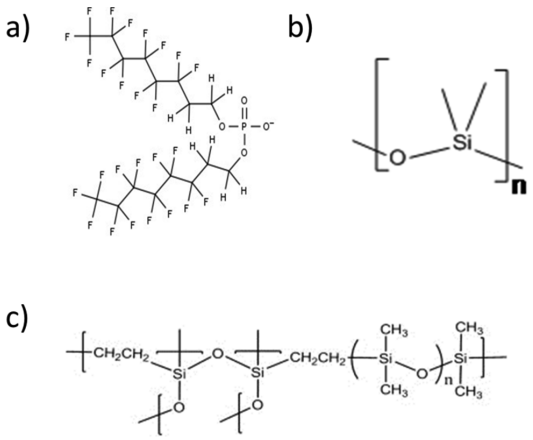

Figure 11. The used functionalizing agents. a) The fluorosurfactant Capstone FS-63. b) The repeating unit of polydimethylsiloxane (PDMS). c) Cross-linked PDMS network [81].

A cross-linked polydimethylsiloxane (PDMS, Dow Corning Sylgard 184) solution was prepared by first mixing a two-part commercial PDMS, consisting of a base component and a cross-linking curing agent in the ratio 10:1, which was then diluted in toluene (Sigma Aldrich) to form a 10 wt-% solution. Faceal Oleo HD (Uudenmaan Pintasuojaus, Finland), a commercial water-repellent protective agent consisting of waterborne acrylic copolymer with fluorinated groups for hydro- and oleophobicity, non-ionic cross-linking groups and silane groups for bonding to mineral surfaces, was used as received as a reference coating to evaluate the effectiveness and performance of the PDMS coatings on granite.

4.2. Protective application techniques

4.2.1. Functionalization through total immersion

Functionalization of marble stones through a total immersion technique was performed by using solutions with known concentrations produced by dilution in Milli-Q purified water, ethylene glycol and co-solvents solutions consisting of water combined with ethylene glycol, ethanol, methanol or propylene glycol. Typically, three marble pieces per treatment were put into beakers containing 40 mL of the selected hydrophobization mixture at different concentrations when diluted in a solvent. The reaction vessels were sealed and put into a temperature-controlled oven for a specific reaction time. After the total immersion functionalization, the samples were washed with water and dried at 60 °C for another 24 h. The marble samples were then kept at room temperature for a week before any experiments were performed. The investigated reaction ranges on marble through the total immersion method are summarized in Figure 12 and Table 1.

Table 1. Samples produced to investigate the static system – application parameters.

Sample	Solvent used	Co-solvent ratio	Functionalization temperature	Reaction time	Surfactant concentration by volume
M_a-1h-1%	H_2O	-	60 °C	1 h	1%
M_a-1h-5%	H_2O	-	60 °C	1 h	5%
M_a-1h-10%	H_2O	-	60 °C	1 h	10%
M_a-24h-1%	H_2O	-	60 °C	24 h	1%
M_a-24h-5%	H_2O	-	60 °C	24 h	5%
M_a-24h-10%	H_2O	-	60 °C	24 h	10%
M_a-72h-1%	H_2O	-	60 °C	72 h	1%
M_a-72h-5%	H_2O	-	60 °C	72 h	5%
M_a-72h-10%	H_2O	-	60 °C	72 h	10%
M_b-W-20C	H_2O	-	20 °C	24 h	10%
M_b-W-40C	H_2O	-	40 °C	24 h	10%
M_b-W-60C	H_2O	-	60 °C	24 h	10%
M_b-W-80C	H_2O	-	80 °C	24 h	10%
M_b-25EG-20C	EG - H_2O	25:75	20 °C	24 h	10%
M_b-25EG-40C	EG - H_2O	25:75	40 °C	24 h	10%
M_b-25EG-60C	EG - H_2O	25:75	60 °C	24 h	10%
M_b-25EG-80C	EG - H_2O	25:75	80 °C	24 h	10%
M_b-50EG-20C	EG - H_2O	50:50	20 °C	24 h	10%
M_b-50EG-40C	EG - H_2O	50:50	40 °C	24 h	10%
M_b-50EG-60C	EG - H_2O	50:50	60 °C	24 h	10%
M_b-50EG-80C	EG - H_2O	50:50	80 °C	24 h	10%
M_b-75EG-20C	EG - H_2O	75:25	20 °C	24 h	10%
M_b-75EG-40C	EG - H_2O	75:25	40 °C	24 h	10%
M_b-75EG-60C	EG - H_2O	75:25	60 °C	24 h	10%
M_b-75EG-80C	EG - H_2O	75:25	80 °C	24 h	10%
M_b-100EG-20C	EG	-	20 °C	24 h	10%
M_b-100EG-40C	EG	-	40 °C	24 h	10%
M_b-100EG-60C	EG	-	60 °C	24 h	10%
M_b-100EG-80C	EG	-	80 °C	24 h	10%
M_c-25PG	PG - H_2O	25:75	60 °C	24 h	10%
M_c-50PG	PG - H_2O	50:50	60 °C	24 h	10%
M_c-25Me	MeOH - H_2O	25:75	60 °C	24 h	10%
M_c-50Me	MeOH - H_2O	50:50	60 °C	24 h	10%
M_c-25Et	EtOH - H_2O	25:75	60 °C	24 h	10%
M_c-50Et	EtOH - H_2O	50:50	60 °C	24 h	10%

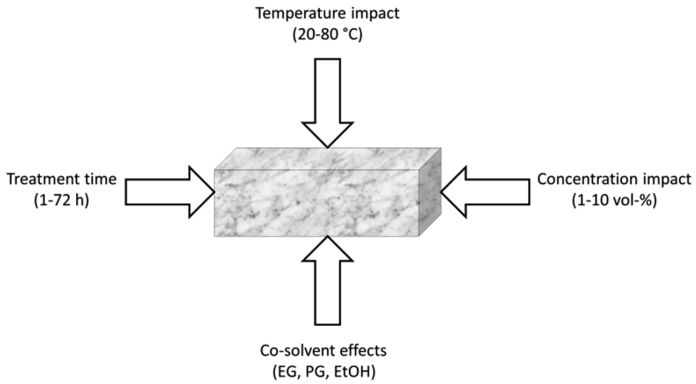

Figure 12. Investigated reaction ranges for marble.

4.2.2. Functionalization through spray coating

Functionalization of marble stones via spray coating was performed by using an optimized concentration of the fluorosurfactants (10 vol-%). Dilutions were made using water and varying concentrations of two suitable co-solvents for the system, water combined with ethylene glycol and ethanol.

A volume of 100 mL/m^2 of all the solutions was applied to the stones using a custom made spray coater (Arctic IP Investment Ab, Salo, Finland) with variable pressure, flow rate, and pitch. To apply 100 mL/m^2, a flow rate of 1.05 mL/min was used with an application speed of 35 mm/s, a pitch of 5 mm, a pressure of 1 bar and a spray-head-to-surface distance of 200 mm. The used spray head was a DAGR airbrush (Devilbiss, Dorset, United Kingdom). After coating, the samples were allowed to react for 24 hours at room temperature, after which the samples were placed in a 60 °C oven for 24 hours. The marble samples were then kept at room temperature for a week before any experiments were performed. The exact reaction conditions for the spray coated marble samples discussed in this thesis are summarized in Table 2.

Table 2. Samples produced to investigate the dynamic system – application parameters. All samples were prepared at a surfactant concentration of 10 vol-% at 25 °C and were allowed to react for 24 h.

Sample	Solvent used	Co-solvent ratio
M_d-W	H_2O	-
M_d-25EG	$C_2H_6O_2$ - H_2O	25:75
M_d-50EG	$C_2H_6O_2$ - H_2O	50:50
M_d-100EG	$C_2H_6O_2$	-
M_d-25Et	C_2H_5OH- H_2O	25:75
M_d-50Et	C_2H_5OH- H_2O	50:50

For the granite samples, the same spray-coater was used to apply the PDMS solution and the commercial silane Faceal Oleo HD on granite stones. By varying the spray-head speed, 20-100 mL/m^2 of the 10 wt-% PDMS in toluene solution were applied to the granite stones, while using the flow rate of 0.2 mL/min, a pitch of 2 mm, a pressure of 2 bar and the spray-head to surface distance of 330 mm. 400 mL/m^2 of the Faceal Oleo HD solution was applied as received, using a spray-head speed of 30 mm/s, a flow rate of 0.5 mL/min, a pitch of 2 mm, a pressure of 1 bar and a spray-head to surface distance of 330 mm. After coating, the granite samples were allowed to react for a week at room temperature before any experiments were performed. The exact reaction conditions for the spray-coated granite samples discussed in this thesis are summarized in Table 3.

Table 3. Samples produced for granite studies – application parameters. All samples were prepared at 25 °C and were allowed to react for 24 h.

Sample	Component used	Surface coverage [mL/m^2]	Component concentration [Mass-%]
G-PDMS-20	PDMS	20	10
G-PDMS-40	PDMS	40	10
G-PDMS-60	PDMS	60	10
G-PDMS-80	PDMS	80	10
G-PDMS-100	PDMS	100	10
G-FO-400	Faceal Oleo HD	400	100[6]

[6] As received. The dry weight of the commercial Faceal Oleo HD solution was experimentally determined to be 3.70±0.06%

5. Characterization methods

5.1. Capillary water absorption

Capillary water absorption is one of the most important parameters to consider in stone conversation research. It is a powerful parameter that can be used to evaluate how much a functionalization affects the water absorption capacity of natural stones. As many of the weathering effects discussed in Chapter 2.2 are dependent on water absorption, a capillary absorption measurement can be used to quickly evaluate and predict the functionality of a protective functionalization.

Capillary water absorption measurements were performed according to a method adapted from the current standard [82]. Measurements were carried out for at least 48 h, ensuring that the water absorption through capillary forces reached a maximum value. The capillary absorption was calculated according to:

$$Q_{CA} = \frac{\Delta m}{A} = \frac{m_x - m_0}{A}, \quad (14)$$

where Q_{CA}, the amount of water absorbed per unit area, m_x, by capillarity (in kg/m^2), is calculated by considering the mass difference the sample expresses at time x, when compared to the starting mass, m_0, normalized against the area of the surface in contact with the filter paper bed, A (in m^2). Relative absorption values were further obtained by:

$$\%_{Abs} = \frac{Q_{samples}^{48\,h}}{Q_{STD}^{48\,h}} \times 100\%. \quad (15)$$

The obtained averaged capillary absorption data for the functionalized samples after 48 h on the wet bed, $Q_{samples}^{48\,h}$, was further normalized against the average value obtained from several untreated samples of the same dimensions, $Q_{STD}^{48\,h}$, thus giving a value in percent absorption, $\%_{Abs}$, compared to the untreated stones at the given time point. The normalized absorption value was then subtracted from 100% resulting in the water protection efficiency of the stone. The use of three stone pieces per coating and measurement thus provided the standard deviations seen in the presented water protection efficiency tables and figures.

5.2. Appearance – color coordinates

The potential optical effect the treatments had on the natural stones was investigated through colorimetric measurements using a Minolta CM3600d

spectrophotometer (Konica Minolta, Marunouchi, Chiyoda, Tokyo, Japan) and evaluating the absolute color difference, ΔE^*_{ab}, in the CIELAB color space, with ΔE^*_{ab} defined as [83]:

$$\Delta E^*_{ab} = \sqrt{(L^*_2 - L^*_1)^2 + (a^*_2 - a^*_1)^2 + (b^*_2 - b^*_1)^2}, \quad (16)$$

where L_2 is the lightness of the standard sample and L_1 is the lightness of a processed sample. The same annotation also applies for a (the red-green color component), and b (the blue-yellow color component).

5.3. Water vapor permeability

The water vapor permeability is generally studied by attaching treated and untreated stones to a container with water and weighing the system once every 24 h [12]. A slightly modified setup was used in the experiments presented in this thesis. A cylindrical piece of stone is sealed into the top of a plastic tube (d = 30 mm) with an elastomeric polymer, PDMS, Sylgard 184 from Dow Corning, and the water vapor permeability was studied over time gravimetrically. The measurements were carried out at a relative humidity of 51.5±4%. The measurement system is illustrated in Figure 13.

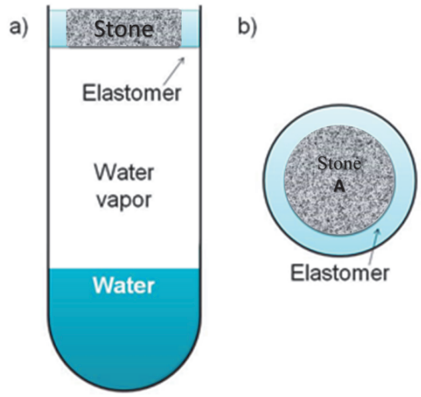

Figure 13. a) Experimental setup of the water vapor permeability tests used in this thesis, b) stone with known top area (=A).

The water vapor permeability rate was calculated by:

$$Q_{perm.} = \frac{\Delta m}{A} = \frac{m_{t_i} - m_{t_0}}{A}, \quad (17)$$

where $Q_{perm.}$ is the water vapor penetrated per unit area (in mg/cm²), Δm is the mass difference between m_{t_0}, the mass of the whole system at the time t_0 (in mg),

and m_{t_i}, the mass of the whole system at the time t_i (in mg). A is the surface area (in cm^2) of the schematic sample shown in Figure 13. The water vapor penetration was plotted against time to evaluate the effect the different coatings had on this important property.

5.4. Contact angles

A high static contact angle (SCA) is considered as a prerequisite for a good hydrophobic treatment, as a successful surface functionalization is needed to inhibit water absorption. The contact angle can be calculated from the interfacial tensions that exist within a solid-liquid-vapor system. These interfacial tensions are represented by the arrows in Figure 14.

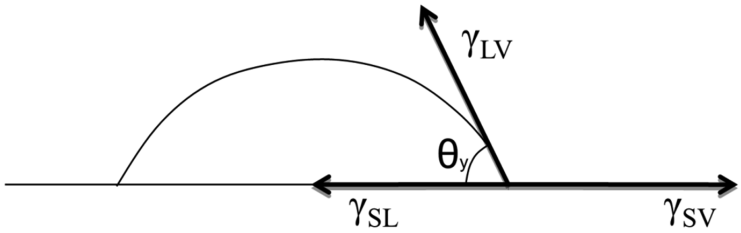

Figure 14. A liquid droplet on a solid surface, with the interfacial tensions shown.

The equation that describes the connection between the contact angle, θ_Y, and the interfacial tensions shown in Figure 14 is known as the Young equation [84]:

$$\gamma_{SV} = \gamma_{LV} \cos\theta_Y + \gamma_{SL}\,, \tag{18}$$

where γ_{SV} is the solid-vapor interfacial tension, γ_{LV} is the liquid-vapor interfacial tension, γ_{SL} is the solid-liquid interfacial tension and θ_Y is the Young contact angle. There are several types of contact angles that could be measured, e.g. the static, receding and advancing contact angle. However, the data obtained would not give much further useful information linked to the effectiveness of the surface treatments when stone protection is concerned. In this thesis, water contact angles were measured using a KSV CAM 200 optical goniometer (KSV instruments Ltd., Helsinki, Finland), using 2 μL droplets of Milli-Q purified water that were applied by a microsyringe in triplicate for each sample, thus providing the reported standard deviations.

5.5. Dynamic light scattering

When the size and size distribution of particles or micellar aggregate systems are to be determined (typical measurement range 0.3 nm–10 μm), dynamic light scattering (DLS) is one of the fastest methods available. DLS measures temporal fluctuations of scattered light, which occur as a consequence of the Brownian motion of particles in a solution. The temporal variations of the scattered light yield a Doppler shift and a broadening of the central Rayleigh line which can be used to determine the dynamic properties of the system and convert the obtained data to a particle size [85]. By considering the Brownian motion of particles, which travel at a certain speed, the hydrodynamic size of the particles can be related to the movement via the Stokes-Einstein equation:

$$D = \frac{k_b T}{6\pi\eta d_h}, \tag{19}$$

where D is the diffusion coefficient, k_b is the Boltzmann constant, η is the solvent viscosity, T is the absolute temperature and d_h the hydrodynamic diameter.

In DLS, a well-defined light beam, usually a monochromatic laser beam, is used to illuminate particles that induce light scattering, such as micellar aggregates or vesicles in a solution. The initial position and scattering of the analyzed particles at the time t is then compared to another signal obtained at the time $t + \tau$ in a process called correlation. This correlation is a mathematical method used to measure how a system changes over time and evaluate the non-random nature of a system in an apparently random dataset. When using a temporal intensity trace in DLS analysis, the correlation coefficient, $G(\tau)$, can be calculated as [86]:

$$G(\tau) = \int_0^\infty I(t)I(t+\tau)dt\ , \tag{20}$$

where t represents the initial time and τ the delay time. This can be simplified to a summation:

$$G_k(\tau_k) = \sum_{i=0} I(t_i)I(t_i + \tau_i). \tag{21}$$

To better explain this process, an example is provided in Figure 15. All particles are as in the starting point at time t and the correlation is perfect (=1). The blue particles have moved (arrows) at time $t + \tau$ *(e.g. 80 μs)* and the correlation could be for instance 0.85. An implication of this is that the faster a correlogram reaches zero, the faster the analyzed particles are and consequently have a larger diffusion in the solution or potentially they aggregate, sediment or flocculate. From this follows that correlograms with a low starting value have very fast particles (= fast diffusion or sedimentation/flocculation). In a DLS analysis, the correlation

software compares the initial state with later states. If the states are identical, the correlation obtained is 1. The chance of perfect correlation is of course only possible in the first microseconds of a measurement, as the continuous movement of water molecules induces diffusion of all particles.

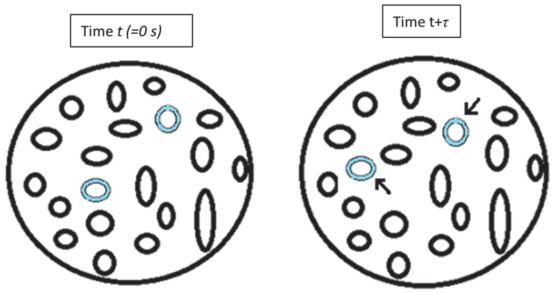

Figure 15. Particles in the laser path at time t and time t + τ.

In a real measurement, a correlation close to 1 is desirable, as it would indicate the best qualitative result. As a rule of thumb, correlation values around 0.8 and above imply results with excellent quality, while results with correlation values below 0.8 are indicative of decreasing quality. The results can, however, be acceptable if a sufficiently long correlation time is used, as the results depend on baseline noise and signal intensity. As longer correlation times provide more data, the signal intensity will gradually accumulate to finally overcome the baseline noise, resulting in a better signal-to-noise ratio, thus providing reliable results even for systems with very low correlation values.

Another parameter that can be studied using DLS is the impact that temperature variations and different solvents have on the relative concentration of micellar aggregates. This parameter was studied by multiplying the size distribution with the derived count rate, i.e. the scattered intensity after correction for the used attenuator, eliminating effects from temperature and viscosity and providing comparable data for the studied datasets. By using the derived count rate, a parameter linked to the concentration of micellar aggregates [87-91], a semi-quantitative analysis of the changes in both concentration and size distribution at different temperatures was possible.

The instrument used to measure dynamic light scattering was a Zetasizer Nano ZS (Malvern Instruments, Malvern, United Kingdom). Along with particle size distributions, the machine gives a cumulant mean value, called z-average. This z-average value is obtained based on the signal intensity fitted to a polynomial of the natural logarithm of the G1 correlation function according to:

$$Ln[G1] = a + bt + ct^2 + dt^3 + et^4 + \cdots, \quad (22)$$

where the value of b is the z-average diffusion coefficient, which is converted into a size using the dispersants viscosity and instrument constants. Only the terms a, b and c are used by the Malvern software for z-average calculation to avoid over-resolving the data.

5.6. Viscosity

Several methods can be used to measure the viscosity of a fluid, such as Ostwald viscometers and rotational rheometers [92]. To study the fluorosurfactant solutions used to produce the M_b sample series, a Bohlin CS rotational rheometer (Bohlin reologi AB, Lund, Sweden) was used, as illustrated in Figure 16.

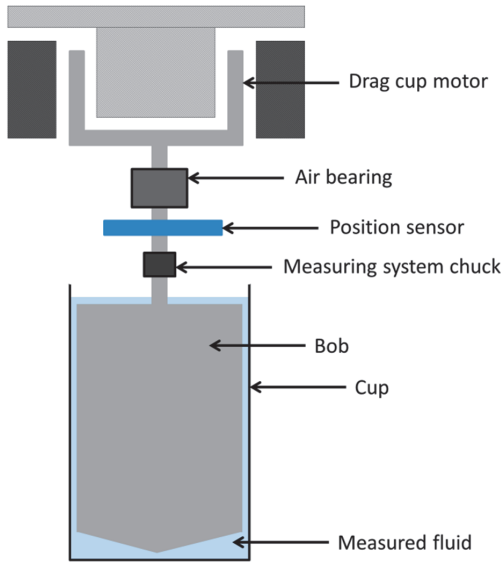

Figure 16. The used measurement setup of the Bohlin CS rheometer. Adapted in part from [92].

The fluorosurfactant solutions were added to the temperature-controlled cup. The rotating bob was then inserted and rotated at set shear rates to determine the viscosity as a function of temperature via the temperature-controlled cup.

5.7. Determining the effective pore hydrophobization depth

A novel method was developed to investigate how deep the marble functionalizations were effective at preventing water absorption. This method is illustrated in Figure 17.

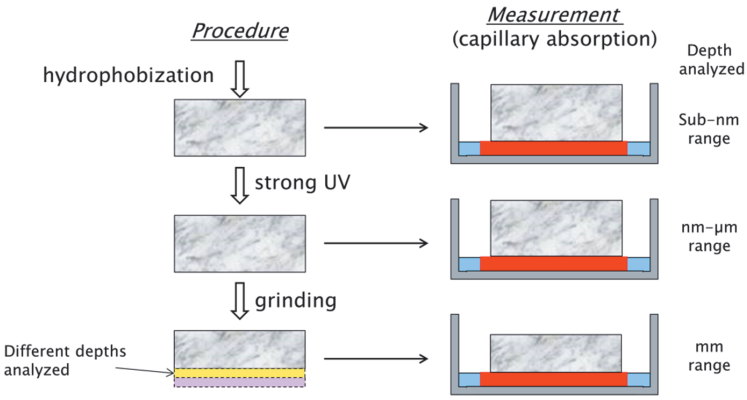

Figure 17. Method used to determine effective functionalization depth.

Initially, after coating, the capillary absorption is recorded to obtain indicative results of the coating performance at a sub-nanometer level. The next step is to intentionally degrade the outermost surface functionalization by using a strong UV light[7]. To remove the outer surface functionalization of a typical sample, 30 minutes of UV irradiation was needed. The surface degradation was subsequently confirmed by contact angle measurements, followed by capillary absorption to investigate functionality at the nm-µm range. The micrometer range was reached through the limited penetration of UV light into marble. The next step in the depth analysis study was to use a belt and disk grinding machine (Biltema, Helsingborg, Sweden) to remove 0.5, 1.0 and 2.0 mm through grinding[8] of the outermost marble surface, permitting the produced surface to be investigated by the capillary absorption method at the millimeter range.

5.8. Testing anti-graffiti performance

Two commercial graffiti spray paints from Montana-Cans (Heidelberg, Germany) were used for graffiti resistance testing of the spray-coated marble samples (M_C series). Montana Black, a solvent-based lacquer consisting of nitrocellulose and alkyd resin-based color with evaporation-driven drying and Montana White, a synthetic lacquer of alkyd resin basis with oxidizing drying were used in the tests. According to the product specification, the solvents used in both products were xylene, acetone, butane, propane, 2-methoxy-1-methylethyl acetate, ethylbenzene and solvent naphtha. Incidentally, both the selected colors appeared black when

[7] A VZero 085 UV lamp from Integration Technology Ltd with an arc length of 85 mm and a power output of 200 W/cm was used in these experiments

[8] The grinding depth was determined using a digital caliper with an accuracy of 0.01 mm

applied to marble, thus offering the best color contrast available for the visual and computational analyses.

The graffiti color was applied on the stones in the M_c series in even layers using a cardboard mask until the selected areas were covered, after which the painted stones were allowed to dry for 24 h at room temperature according to the scheme presented in Figure 18. The cleanability was tested by pressure washing the soiled surfaces with a low-cost pressure washer, a Kärcher K2 (Alfred Kärcher GmbH & Co. KG, Winnenden, Germany) with a maximum pressure of 11 MPa, for 5 min with the pressure washer sprayhead at a distance of 10 cm from the surface for each stone. To quantify the cleanability of the samples, the following color analysis method was developed; a cardboard box (40x40x40 cm^3) with even LED lighting was constructed. A digital camera was attached to an opening at the top of the box and photographs were taken of the samples before and after each graffiti cleaning cycle. The ImageJ software (version 1.48v) was then used to calculate the pixel surface area of the areas covered by each graffiti color. Due to the excellent black and white contrast offered by black graffiti on white marble, the pixel area difference in percentage could be calculated.

After the cleanability evaluation, the remaining color was removed with a tissue soaked in acetone until the surfaces appeared clean with no traces of the previously applied color. A new layer of paint was then applied on the same area as the previous layer after which the washing and evaluation were repeated. Note that the acetone cleaning steps did not affect the functionalization (see Paper **III** for further details).

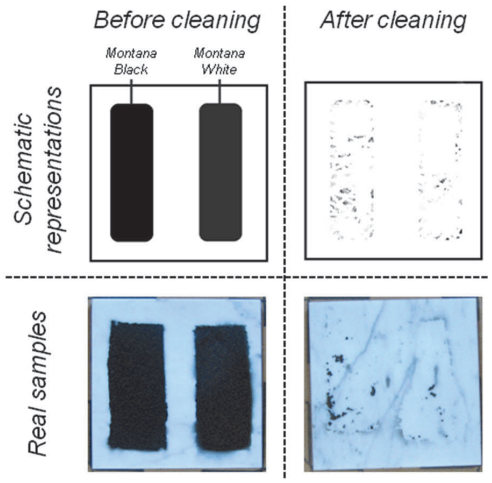

Figure 18. Color application scheme, before and after cleaning, with schematic and real samples.

5.9. Simulation of aging effects

5.9.1. Acid degradation

Hydrolysis is one of the main processes by which granitic rocks are chemically weathered. Granite stones with the dimensions of 5x5x1 cm^3 were used to evaluate the effects of acid degradation on pure granite as well as the PDMS coatings and the reference Faceal Oleo HD coating. The stones were immersed in a solution with the initial concentration of 0.001 M (pH 3) HCl solution for 1 month (30 days), using 3 mL acid per gram stone. The solution was changed every 7 days, to ensure a continuous hydrolysis. The pH of the reacted solution was measured every week to monitor changes, investigating if H^+ was consumed and if hydrolysis continued throughout the experiment. It was found that, for all samples, the pH increased to 3.3-3.5 after each week. After the acid immersion exposure, the stones were evaluated with contact angle and capillary absorption measurements, and through determination of mass loss.

5.9.2. Frost weathering

The freeze-thaw test attempts to reproduce the stresses, which may arise inside the rock when water turns into ice, generating pressure on the rock material. These effects are generally obtained by varying the temperature below and above 0 °C in the samples containing water. The freeze-thaw test was conducted in a way adapted from [93] (see Figure 19). The water-saturated samples were left to freeze at −18 °C for 16 h and then allowed to thaw at 40 °C for another 8 h. This process is defined as one freeze-thaw cycle and was repeated 30 times in this experiment. The effects of the freeze-thaw cycling were evaluated by measuring color difference, contact angles, capillary absorption and the weight loss after the last cycle.

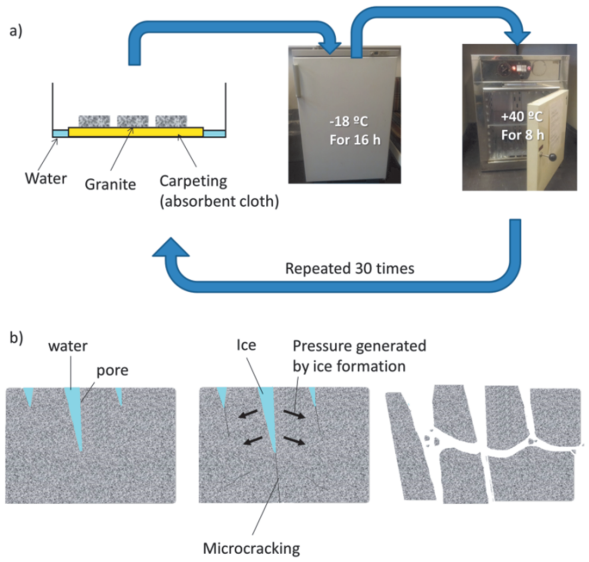

Figure 19. Schematic of the frost weathering a) cycling process and b) mechanism of degradation.

5.9.3. Salt weathering – resistance to salt crystallization

When investigating the impact that salt weathering has on natural stones, the common way of testing is to immerse the stone in a salt-containing solution for a set time, dry the stone and repeat the process [36]. While this is an excellent way of testing the impact of consolidating treatments, which block the stone pores and thus salt ion diffusion into the stone from all sides, it is not suitable for the evaluation of protective coatings only covering one face of the stone, as in the case of the PDMS-coated granite stones presented in this thesis. This is accounted for by exposing stones with different protective treatments to capillary absorption of salt solutions, thus only exposing the protected side of the stone to the degrading effects of salt crystallization. The test was carried out by performing a 'salt exposure' – 'drying' cycle as follows; 1) capillary absorption of a 14 wt-% sodium sulfate solution for 2 h by placing the treated side of the stones facing the absorbent bed, 2) oven drying at 40 °C for 8 h, and 3) cooling at room temperature for 14 h. After every 5 cycles, the tested stones were washed in for 3 days (with continuously renewed water), after which the stones were dried to constant weight. The effects of the salt crystallization were evaluated by measuring the weight loss (every 5 cycles) and by measuring color difference, contact angles and capillary absorption after the 30th and final cycle.

5.9.4. Standardized accelerated aging

To test the long-term impact of UV light and moisture on the coated granite stones, the samples were exposed to standardized accelerated aging using a QUV Accelerated Weathering Tester (Q-lab, Ohio, USA), which is capable of reproducing the damaging effects caused by sunlight (= photodegradation) and the damaging effects of dew and rain (= chemical weathering).

The QUV Accelerated Weathering Tester reproduces the sunlight and moisture-driven effects by exposing the tested materials to alternating cycles of UV light and moisture at controlled, elevated temperatures. These features allow the QUV Accelerated Weathering Tester to reproduce the damage that corresponds to several months or years of real life outdoors exposure in a few weeks.

In the test, the samples were exposed to UV irradiation for 8 h, followed by 4 h of water condensation. This test was carried out for 2 months, which according to the European standard [94] would correspond to two years of actual outdoor exposure. The effects of the accelerated UV and moisture driven weathering (UV/M weathering) were evaluated by measuring color difference, contact angles, capillary absorption and weight loss.

6. Results and discussion

6.1. Marble protection via fluorosurfactant functionalization – static systems

6.1.1. Static systems – effects of time and volume

The first step taken in order to understand the properties affecting the functionalization efficiency of fluorosurfactants on marble was to investigate the influence fluorosurfactant concentration and functionalization time had on the hydrophobic properties of stones modified with FS-63 in total immersion functionalizations. This was achieved by studying the functionalizations in the M_a series.

Static water contact angle measurements were carried out to study how well the outermost stone surface had been hydrophobized (summarized in Table 4). While the pure marble surface had a contact angle of about 64°, the water contact angles for the modified samples were in the range of 95-105°, which shows that the FS-63 functionalizations gave a complete surface coverage for the as-treated samples relatively quickly (within 1 h) irrespective of the solution concentration.

Table 4. Water contact angle values and protection efficiency values (relative to pure marble stones) before and after 30 min of UV treatment.

Sample	**Water contact angle [°]**		**Protection efficiency [%]**	
	As recieved	After UV	As recieved	After UV
Pure marble	64±3	17±2	0±10%	0±10%
	After treatment	After UV	After treatment	After UV
M_a-1h-1%	105±3	40±10	35±2	19±3
M_a-1h-5%	95±1	74±6	76±8	38±4
M_a-1h-10%	99±8	48±6	89±7	34±8
M_a-24h-1%	97±3	78±3	99±4	29±5
M_a-24h-5%	100±1	58±7	100±0	80±10
M_a-24h-10%	102±3	79±5	100±0	100±3
M_a-72h-1%	100±3	89±3	90±20	0±10
M_a-72h-5%	102±2	66±6	100±0	80±20
M_a-72h-10%	101±3	42±10	100±0	99.4±0.5

A more robust evaluation method is the capillary absorption test, in which the functionalized marble stones are continuously in direct contact with a water bed for a prolonged period of time. Increasing the FS-63 concentration during functionalization correspondingly improved the water protection efficiency for all

the studied systems, revealing that the functionalization process is concentration-dependent. For the samples functionalized for 1 h (the M_a-1h series), the water protection efficiency increases from 35%, through 76%, to ~90% with increasing functionalization concentration (from 1 vol-% to 5 vol-%, and finally to 10 vol-% FS-63). The treatment time is an equally important parameter, as an increase from 1 h to 24 h or 72 h resulted in a fully protected surface for all of the investigated concentrations. These results are summarized in Figure 20.

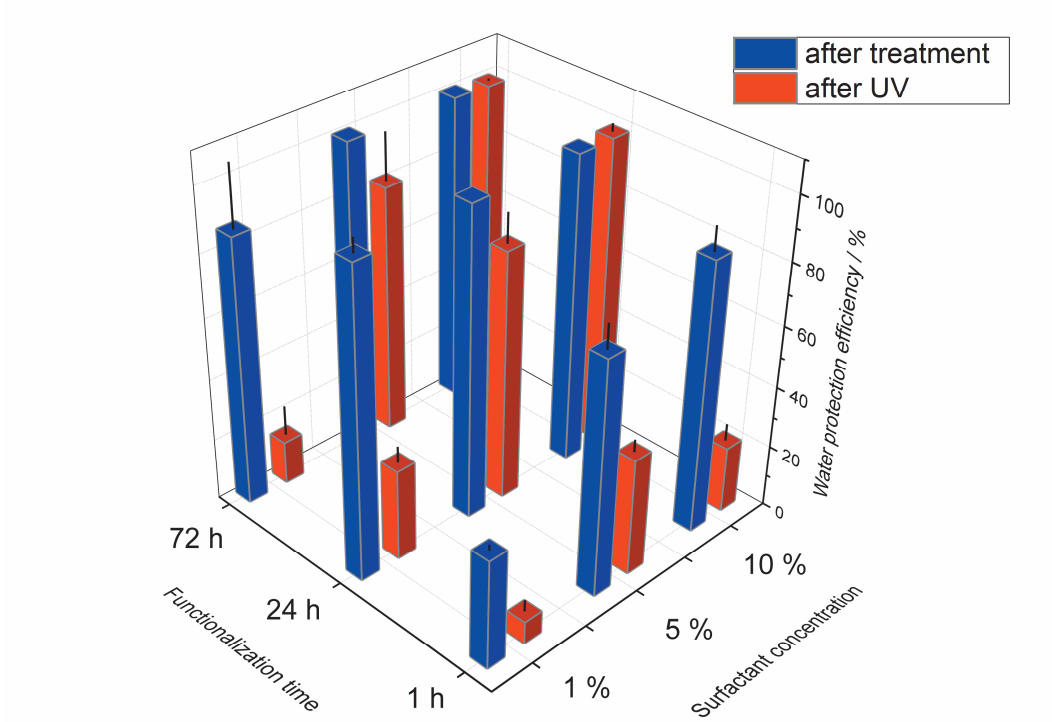

Figure 20. Water protection efficiency for the FS-63 formulation in a concentration-reaction time matrix.

As expected, the treated stones did not perform equally well after strong UV exposure for 30 min, due to varying pore functionalization degrees. The lowered contact angle values listed in Table 4 indicate that the outermost hydrophobic layer had been removed. Several of the samples that displayed a good water protection efficiency after treatment now displayed water protection efficiencies of less than 40% water, which is true for all functionalizations performed with too short reaction time or too low surfactant concentration, while the samples treated with a 5 vol-% FS-63 solution for 24 h and 72 h showed an acceptable water protection (above 80% compared to the untreated marble). However, if a

concentration of 10 vol-% was used, a close to complete protection was obtained when the stone was treated for at least 24 h, even after UV degradation. This is a good improvement compared to previous studies [12,17,95-98], where the maximum protection efficiency for treated surfaces was 90% after functionalization.

The fact that higher concentrations and longer treatment times improve the hydrophobization of the interior surface of the pore walls implies that the process is kinetically controlled by diffusion of the molecules inside the pores, which will be discussed further in section 6.1.2.2.

The results obtained from the intentional removal of the surface functionalization through severe UV treatments were indicative of an excellent stability for the samples functionalized with FS-63. However, to better estimate the stability of the protective coating over time under natural conditions, accelerated weathering, as specified in 5.9.4, was performed to test the performance of samples functionalized with 5 vol-% FS-63 for 72 h at 60 °C. A test period of 60 days was used in this test.

Before the test commenced, the samples displayed a water protection efficiency of 99.9±0.5% and after 60 days of accelerated weathering, the same samples displayed a water protection efficiency of 80±30% water compared to untreated marble aged for the same amount of time, indicating that the functionalization was reasonably stable. According to [94], the amount of UV radiation the stones are exposed to in the two months of accelerated weathering would correspond to two years of outdoor sun exposure in Helsinki, Finland. Additionally, the water spraying (which simulates rain) will also contribute to the degradation, thus the projected real aging time could be longer.

6.1.2. Static systems – effects of vesicle behavior and temperature

6.1.2.1. Performance of functionalized marble samples

The next step was to investigate the impact that temperature and co-solvent manipulation of possible surfactant aggregate behavior had on the marble hydrophobization efficiency in the total immersion functionalization. This was achieved by studying the functionalization in the M_b series.

Data from the co-solvent and temperature matrix is presented in Table 5 and Figure 21, showing how effective the different solutions were when the treatment was performed at increasing temperatures and when using different EG:water co-solvent ratios.

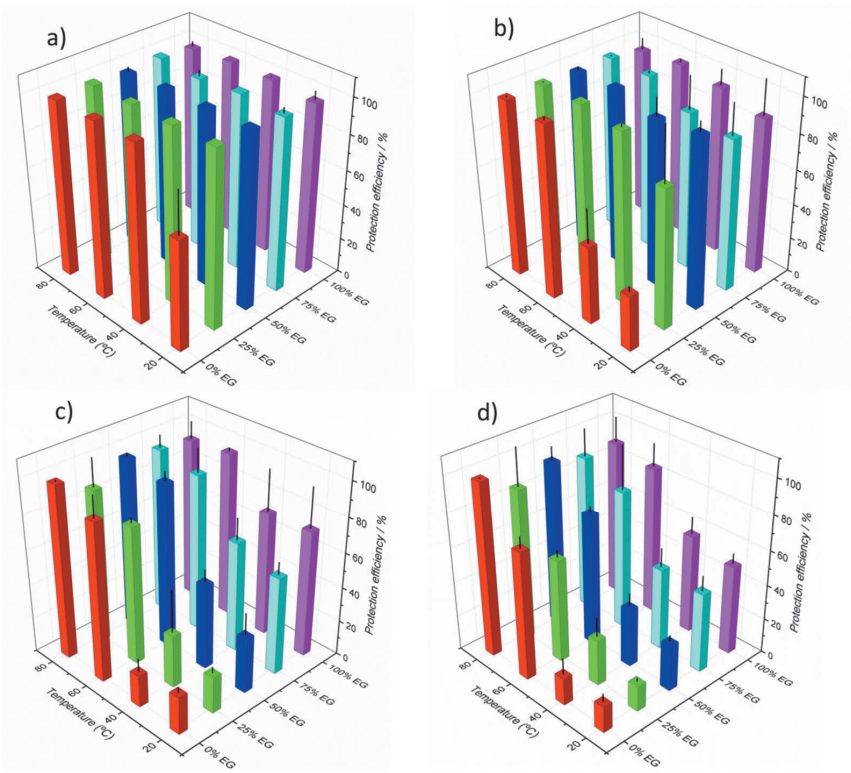

Figure 21. Protection efficiencies recorded for the co-solvent systems at different temperatures after 48 h on the capillary absorption bed. a) After treatment, b) after UV degradation, c) after 1 mm grinding, and d) after 2 mm grinding.

After the functionalization (Figure 21a), the water contact angle for all samples increased from 64±3° for the native marble to 110−120° with no detectable trends, confirming that at least the outermost surface of the marble stones had been successfully functionalized. These contact angle measurements are available in the supplementary data of **Paper II**. In the capillary absorption tests, all treatments (except with 0% EG at 20 °C) performed very well, showing zero or almost zero percent water absorption, and consequently close to 100% protection efficiency. The impact of ethylene glycol addition as a co-solvent can be clearly seen in the 20 °C series, where an addition of only 25% ethylene glycol to the solvent improved the protection efficiency from 60% to 100%. It is important to note also that the higher viscosity in the high EG concentrations did not impact the functionalization negatively and this will be further discussed in Section 6.1.2.2.

Table 5. Protection efficiencies recorded for the various co-solvent systems at different temperatures after 48 h on the capillary absorption bed, after treatment and after UV irradiation and grinding. ± denotes the standard deviation.

Sample	After treatment	After UV	1 mm ground	2 mm ground
Mb-W-20C	60±20	32±3	22±3	15±5
Mb-W-40C	100.0±0.0	40±20	18±8	15±9
Mb-W-60C	100.0±0.0	98±2	90±10	73±7
Mb-W-80C	100.0±0.0	99.7±0.6	99.5±0.9	100±1
Mb-25EG-20C	100.0±0.0	80±30	21±4	15±2
Mb-25EG-40C	100.0±0.0	97±2	30±20	30±10
Mb-25EG-60C	100.0±0.0	99.9±0.2	79±3	59±4
Mb-25EG-80C	100.0±0.0	99.7±0.6	90±20	90±20
Mb-50EG-20C	100.0±0.0	97±6	30±10	27±4
Mb-50EG-40C	100.0±0.0	90±10	49±7	34±7
Mb-50EG-60C	100.0±0.0	100.0±0.0	94±5	75±4
Mb-50EG-80C	99±3	99±2	98±2	94±8
Mb-75EG-20C	98±3	90±20	56±7	45±9
Mb-75EG-40C	100.0±0.0	90±20	60±10	50±10
Mb-75EG-60C	98±3	99±1	90±10	80±20
Mb-75EG-80C	100.0±0.0	99.7±0.5	96±7	90±20
Mb-100EG-20C	97±5	90±20	70±20	51±6
Mb-100EG-40C	99.8±0.4	95±9	70±20	60±10
Mb-100EG-60C	100.0±0.0	98±2	96±2	90±10
Mb-100EG-80C	98±3	96±6	90±10	90±10

After the intentional removal of the outermost functionalization by UV radiation, which was confirmed through contact angle measurements, some clearer trends in the capillary absorption measurements can be observed, as seen in Figure 21b. For treatments performed at 60 °C or higher (independent of EG:water ratio), the stones absorbed close to zero percent water, resulting in protection efficiencies of about 100%. The trends found below 60 °C showed the beneficial effect that ethylene glycol addition had on the protection efficiency, as increasing the EG concentration improved the protection efficiency. The trend was most pronounced in the 20 °C treatment series.

When 1 mm of the outermost surface had been removed, a clear trend was seen in the samples treated at 40 °C and lower. Increasing the ethylene glycol concentration during functionalization correspondingly increased the protection efficiency at 1 mm, which is very interesting, as the higher viscosity imparted by

ethylene glycol during functionalization did not affect the diffusion of the surfactants into the pores negatively. For the samples treated at temperatures above 60 °C, the protection efficiency is relatively high, independent of the ethylene glycol fraction in the solvent. This shows that the impact of increasing the temperature is more significant than the effect of the co-solvent concentration. On the other hand, in practical applications, tuning the solvent properties would be more practical than increasing the temperature. After the final grinding step, when 2 mm of the outermost surface had been removed, the same trends observed in the previous grinding steps were still evident. The trend shows that the beneficial effect of ethylene glycol addition is still present in the treatments performed at 20 °C and 40 °C. At this grinding depth, a distinct improvement in protection efficiency was also observed when increasing the temperature from 40 °C to 60 °C. Both of these effects will be addressed in the following section.

6.1.2.2. Mechanistic studies on temperature and co-solvent effects

In the previous sections, it was observed that increases in the surfactant concentration, reaction time, reaction temperature and the addition of a less polar solvent had positive effects on the protection efficiency even at deeper grinding depths. These parameters can be linked by the Stokes-Einstein diffusion law (equation 19), which governs the flow of particles in a liquid bulk.

Assuming that the diffusion of surfactants forming micellar aggregates follows a Stokes-Einstein diffusion behavior, it can be concluded that an increase in temperature and decrease in viscosity and micellar aggregate diameter will lead to a more rapid diffusion in solutions containing micellar aggregates. The improved protection efficiency at higher temperatures is related to several factors. Beyond the obvious link between diffusion and temperature in equation 19, where higher temperatures give faster diffusion, the temperature also affects the viscosity and possibly also the micellar aggregate size positively, increasing the diffusion of the micellar aggregates.

As can be seen from Figure 22, the viscosity of the studied FS-63 solution mixtures decreases with temperature (generally a decrease of 70−85% when heating from 20 °C to 80 °C), which is beneficial for the diffusion of the potential micellar aggregates.

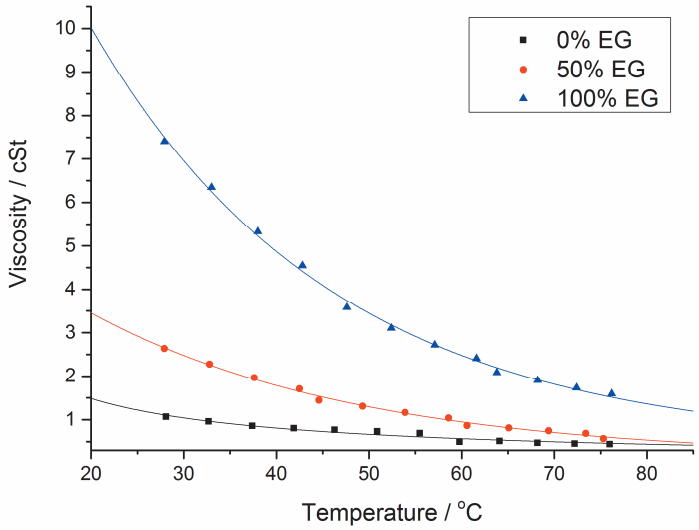

Figure 22. Viscosity as a function of temperature for the different mixtures. The lines are asymptotic fits to the obtained data as a guideline for data interpretation. The solutions 0% EG, 50% EG and 100% EG were used to functionalize the marble stones in the M_b-W, M_b-50EG and M_b-100EG series, respectively.

Dynamic light scattering (DLS) was used to investigate the hydrodynamic diameter (d_h) of the surfactant aggregates in the various solutions. For the solution where FS-63 was diluted in pure water (sample 0% EG), a main peak centered at ~600 nm can clearly be seen (Figure 23). This large vesicle size suggests that the surfactants self-assemble into large unilamellar vesicles (LUV) or multilamellar vesicles (MLV) in aqueous solutions [72]. This is not surprising since the FS-63 fluorosurfactants contain two hydrophobic perfluorinated chains per phosphate head group, resulting in a surfactant packing parameter suitable for the formation of bilayer structures. The presence of large spherical vesicles was further confirmed by light microscopy, where only the largest vesicles (diameter > 1000 nm) could be seen due to the limited resolution. Furthermore, in the DLS size distribution plot, a smaller population of aggregates with a diameter of about 100 nm can also be seen. It is, in any case, clear from the particle size distributions of the vesicles that an increase in temperature causes a decrease in the number of vesicles.

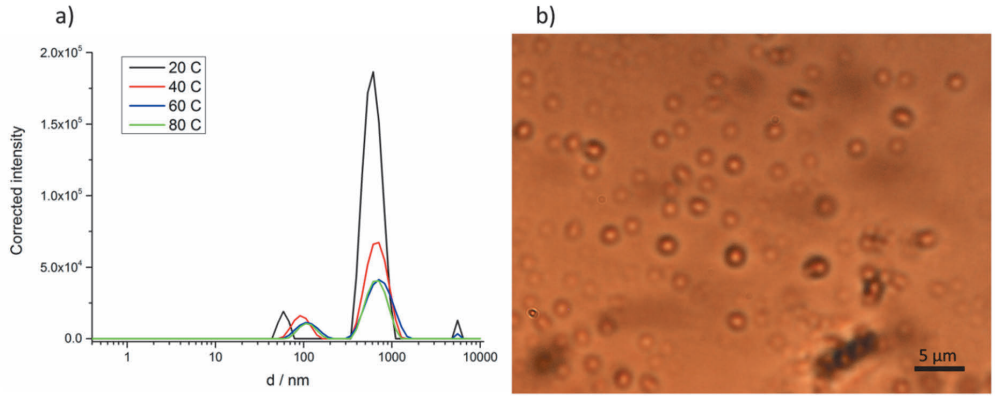

Figure 23. a) Particle (in this case vesicle) size distribution for the 0% EG sample with derived count rate correction. b) Microscopy image showing the surfactant aggregates, confirming the presence of vesicles.

In the capillary absorption tests (Figure 21), a clear improvement in water protection efficiencies could be observed when the EG-to-water ratio was increased already at room temperature. Based on the 1/η behavior in the Stokes-Einstein diffusion equation, one would expect a slower diffusion when adding ethylene glycol to the solution. This is evidenced by the ~5-fold increase in viscosity when exchanging the water with EG (see Figure 22). This indicates that the viscosity of the solution mixture is not a dominating factor for the functionalization process.

The size distributions obtained from the DLS measurements are shown in Figure 24 for the different EG:water ratios, which can be compared to the 0% EG sample in Figure 23a. At 20 °C (black lines), a clear decrease in the size and abundance of the vesicles can be seen, starting from ~600 nm for pure water, moving down to a barely detectable peak at ~100 nm for the pure EG sample (100% EG). Furthermore, looking at the intensities, the amount of vesicles is also decreasing with increasing EG concentration. This effect is due to the change in polarity of the solvent, which destabilizes and/or reorganizes the vesicles [78,79,96]. Consequently there are more free surfactants available in the solutions with high amounts of EG.

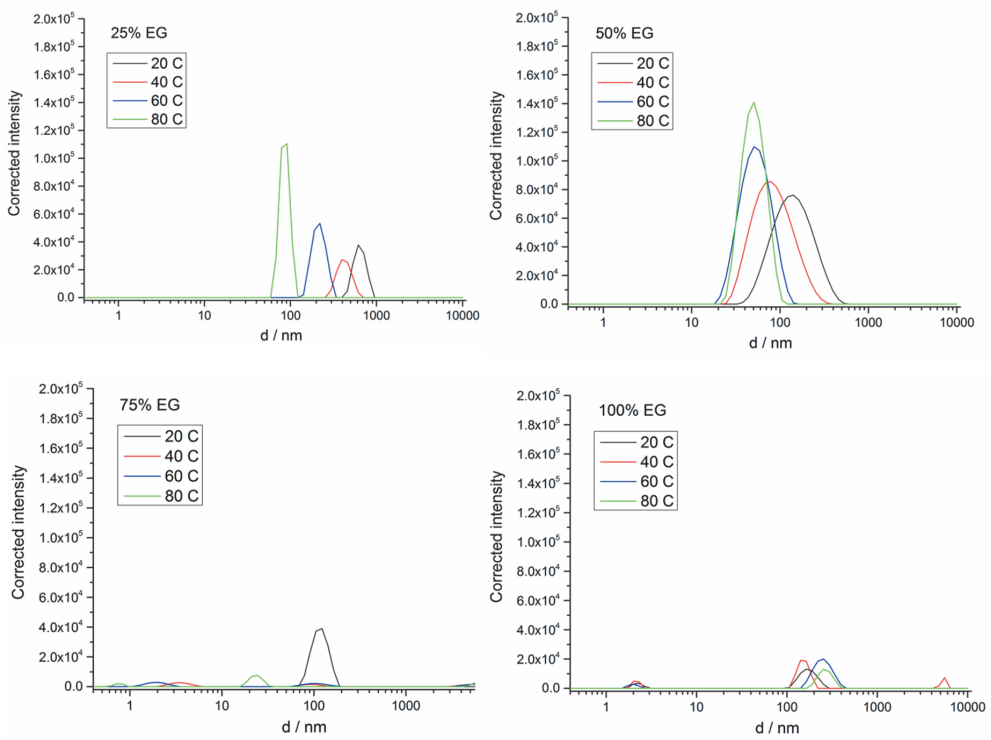

Figure 24. Vesicle size distributions for the various mixtures with derived count rate correction.

In Figure 24, the effect that temperature had on the vesicle behavior at different EG:water ratios is shown. For the 25% EG and 50% EG samples, there is clearly a downshift in vesicle size when increasing the temperature, while the numbers of vesicles are still quite high. Consistent with the Stokes-Einstein equation, the smaller vesicle size also promotes faster diffusion rate which is reflected in Figure 25. This also contributes to the improved protection efficiencies seen for these samples (Figure 21). For the 75% EG and 100% EG samples, an increase in temperature seems to create many small-sized intensity populations in the DLS results, which is difficult to explain. From the DLS correlograms for these samples, an inconsistent behavior was noticed, which is probably related to low vesicle concentrations. This leads to the conclusion that most of the vesicles have broken down into free surfactants under these conditions, which is beneficial for a successful pore functionalization, promoting enhanced diffusion of the surfactant molecules into the pores.

From the DLS measurements, it is also possible to extract the diffusion coefficients as a function of temperature for the solutions containing up to 50% EG, based on the Stokes-Einstein theory (see Figure 25). The increase in

temperature results in faster diffusion rates, which based on the vesicle size distributions seen in Figure 23 and Figure 24 is most likely related to both the disruption of the vesicles and their decrease in size. As the surfactant vesicles completely break down at higher EG concentrations, the Stokes-Einstein assumption cannot be utilized to explain the diffusion phenomenon for the 75% EG and 100% EG series, as there are no observable aggregates. However, free surfactant molecules can diffuse more easily than when they are assembled into micelles or vesicles, as the concentration gradient inside/outside the pores should be the driving force for drawing the surfactants into the pores. There are also additional effects that could contribute to the relatively poor protection efficiencies observed at low temperatures and low EG concentrations. These include the physical hindrance of large vesicles entering the smallest pores (the mean pore diameter of the investigated Carrara marble is 100-400 nm as measured by mercury intrusion porosimetry, see Paper **I** for further details), and the very strong interaction between the phosphate group of the surfactant and the calcium carbonate pore walls of marble which might slow down the diffusion.

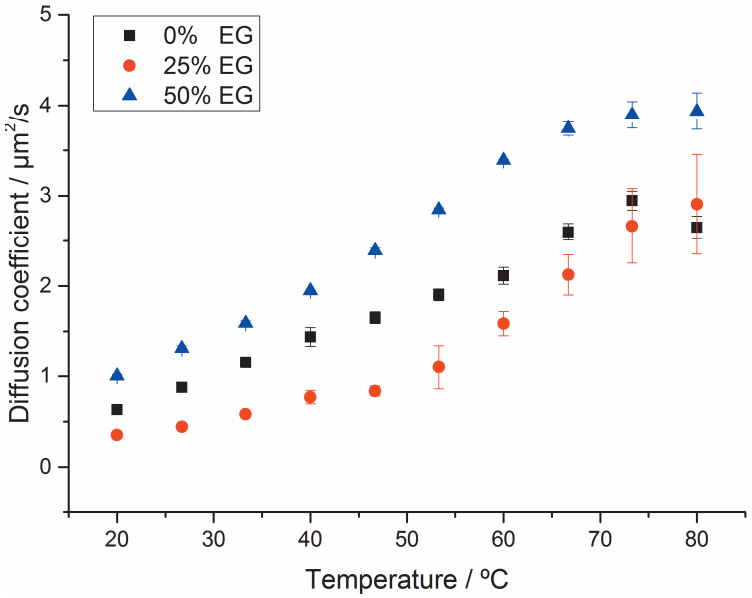

Figure 25. Diffusion coefficients obtained from the DLS measurements.

6.1.2.3. Effect of co-solvent polarity

As lowering the solvent polarity by adding EG to the solvent mixture had a positive effect on the diffusion behavior (and the protection efficiency), potentially other co-solvents could further improve the results. The log Pow value

describes the relative polarity (or solubility properties) of a solvent as the preferential partition a liquid has in octanol and water. On this scale, EG displays a relatively low value (–1.93) [99]. By further increasing the log POW of the co-solvent, i.e. by using propylene glycol (PG, –0.92), methanol (MeOH, –0.74), and ethanol (EtOH, –0.30) under otherwise similar conditions (10 vol-% FS-63 and reaction temperature of 60 °C), it is expected to further favorably influence the micellar behavior of the FS-63 surfactants.

Visual observations and DLS measurements (not shown) revealed that, out of these solvents, only ethylene glycol could be used in its pure form to dilute the FS-63 compound, while when using PG, MeOH or EtOH as co-solvents, the compound started to phase separate at co-solvent-to-water ratios above 0.5. DLS measurements of the solutions containing 25% and 50% co-solvent gave all similar results as the 75% EG and 100% EG solutions, i.e. very poor correlograms and uncertain size distributions most likely due to the collapse of the vesicles. This further proves that the polarity of the solvent plays an important role on the solvation of the hydrophobic perfluorinated chains of the FS-63 surfactant.

Furthermore, the protection efficiencies were evaluated for these samples as well (see Figure 26 and Table 6). The general trend was that the higher log POW the co-solvent has, the better protection efficiency can be achieved. For example, a close to ideal protection efficiency could be obtained for the 25% EtOH, 50% EtOH and 50% MeOH samples even down to a depth of 2 mm, which is a great improvement from the solutions with pure water and EG-water mixtures under similar conditions (see Figure 21 and Table 5). This further corroborates that the disruption of the surfactant vesicles (and possibly also the solution viscosity) plays a crucial role in the functionalization efficiency of porous marble.

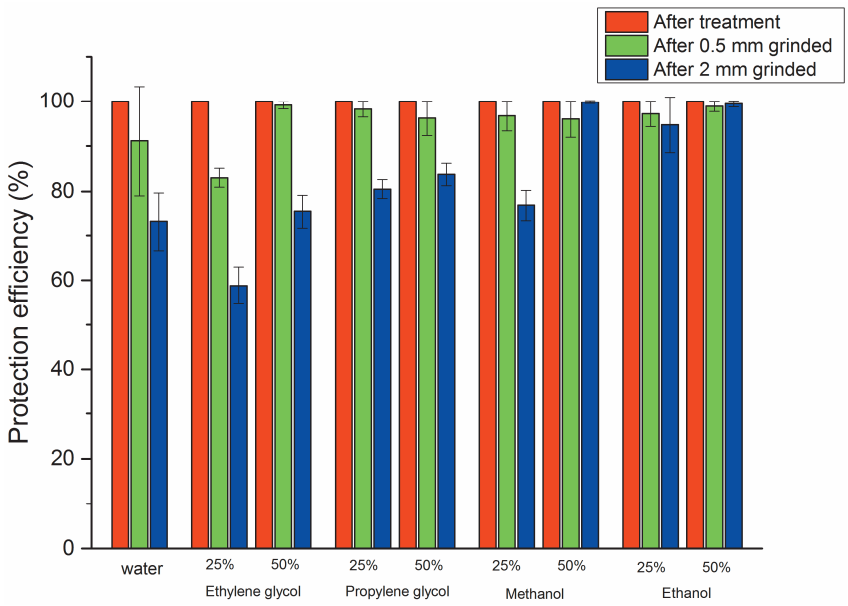

Figure 26. Protection efficiencies for stones in the M_c series after 48 h on the capillary absorption bed. Note that only the added co-solvent is given, while all samples were functionalized at 60 °C, e.g. 25% ethylene glycol corresponds to sample M_c-25EG-60C.

Table 6. Protection efficiencies for stones in the M_c series after 48 h on the capillary absorption bed.

Sample	After treatment	0.5 mm ground	2 mm ground
M_b-W-60C	100±0	90±10	73±7
M_c-25EG-60C	100±0	83±2	59±4
M_c-50EG-60C	100±0	99.1±0.8	75±4
M_c-25PG	100±0	98±2	81±2
M_c-50PG	100±0	96±4	84±2
M_c-25Me	100±0	97±3	77±3
M_c-50Me	100±0	96±4	99.8±0.3
M_c-25Et	100±0	97±3	95±6
M_c-50Et	100±0	99±1	99.4±0.7

6.1.2.4. Water vapor permeability and color change

The water vapor permeability of stone materials should be unchanged by a hydrophobic treatment. This is important as water condensation beneath a protective coating as well as accumulation of condensed water behind a treated stone can lead to stone decay [9]. Water permeability measurements of the stones

functionalized through the protocol immersion functionalization in the Ma-24h series is plotted in Figure 27. The samples display an almost linear increase in $Q_{perm.}$ values as a function of time and the rates are summarized in Table 7.

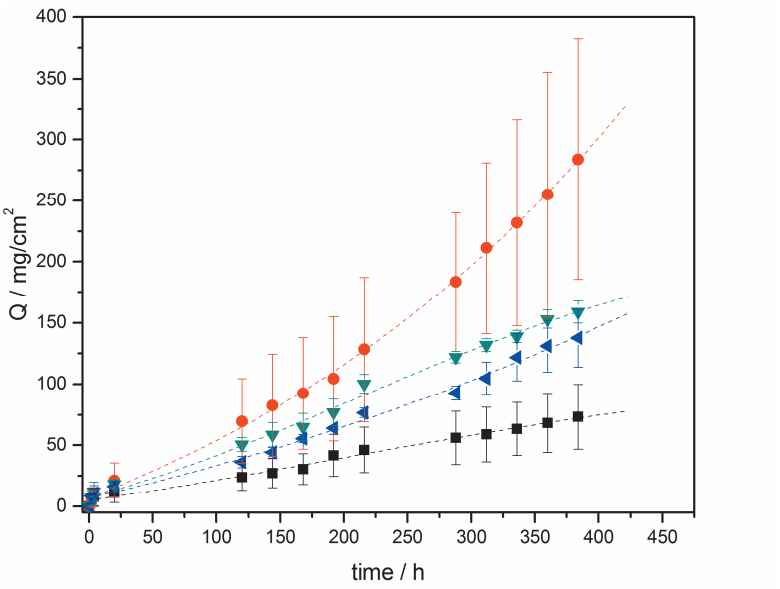

Figure 27. The water vapor permeability rates for marble treated with FS-63 at different concentrations: ■ = untreated, ● = Ma-24h-1%, ▼ = Ma-24h-5% and ◀ = Ma-24h-10%. The dotted lines being the nonlinear regression with a sigmoidal dose-response curve fit are included as guidelines for the eye.

Table 7. The water vapor permeability rates through modified stones as well as the measured color changes after hydrophobization and after UV degradation of all FS-63 treatments when compared to untreated samples.

Sample	Vapor diffusivity rate, Q/t [mg/cm²h]	Color change ΔE^*_{ab}	
		After hydrophobization	After UV degradation
Untreated	0.178±0.005	–	–
Ma-24h-1%	0.69±0.03	3.7	3.6
Ma-24h-5%	0.403±0.001	2.0	3.5
Ma-24h-10%	0.34±0.01	3.3	4.5

The water vapor permeability study yielded very good results; no impediment of the permeability could be detected, indicating that no pore-blocking occurred. This was also the goal of the functionalization, i.e. to apply a layer to the pore walls that would not affect the natural stone negatively. The positive effect of the functionalization on water vapor permeability, i.e. the apparent increase in Q as a function of concentration seen in Figure 27, could be contributed to the increased

hydrophobicity of the marble pores. The diffusion rate of water vapor through hydrophobic pores is greater than the diffusion rate through hydrophilic pores, a phenomenon also encountered in production of hydrophobic nanotubes [100,101] and observed for a similar coating [96]. The reason for the water vapor permeability decreasing again for the highest tested concentration (10 vol-% FS-63) could be due to an increased layer thickness at the pore openings in those pores. However, it should be noted that the permeability for this sample is still higher than for the untreated stones. To further corroborate the non-blocking nature of the surface-lining coating, mercury intrusion porosimetry (MIP) was performed on untreated marble and the sample Ma-5%-24h. No large variations in the open porosity were detected, indicating that the pores are not blocked by the treatment.

Finally, in order to investigate whether any undesired color alterations occurred on the stone surface, colorimetric measurements were conducted on stones treated with different concentrations of FS-63. All hydrophobized samples were compared to untreated stones and this color difference is summarized in Table 7. The small measured color changes ΔE^*_{ab} ~ 2–5) revealed that no significant discoloring of the marble surface had occurred even when using a fluorosurfactant concentration up to 10 vol-%. It should be noted that the detected differences are slightly above the just noticeable difference level, which is defined as the color change needed to see a difference with the naked eye, i.e. ΔE^*_{ab} = 2.3. This is further corroborated by visual comparison between an untreated and functionalized marble stone in Figure 28. The small difference detected in ΔE^*_{ab} was found to be a slight decrease in the lightness parameter (L) when the measured data were evaluated. No additional significant color changes were observed for the UV irradiated samples either.

Figure 28. Untreated (left) marble and marble functionalized with Ma-24h-10% (right) produced for aesthetic evaluation.

6.2. Marble protection via fluorosurfactant functionalization - Dynamic systems

While the studies on static total immersion functionalization systems presented in section 6.1 provide valuable information on the mechanisms of fluorosurfactant functionalization of porous marble systems, the practical applicability of these systems is limited. Thus, a spray coating version of the same functionalization method is presented in this section.

6.2.1. Capillary absorption and contact angles of dynamic system samples

After spray coating, the water contact angles were close to or higher than 90° (Table 8), showing that the spray coating functionalization was successful. While contact angles slightly below 90° were observed for the Md-Et samples, they still displayed significant increases when compared to pure marble. After the graffiti cleaning cycles (see section 6.2.3 for further details), all recorded contact angles had decreased and were below 90°, indicating that the outermost functionalization had been partially removed due to the impact of the pressure washer cleaning. However, all samples still displayed very good results in the capillary absorption tests (Figure 29), showing that the fluorosurfactants had penetrated into the stone. All coatings displayed a large decrease in water absorption. The samples Md-50Et and Md-100EG displayed water protection efficiencies of 98±2% and 96±2%, respectively, while the other samples absorbed almost no water at all, displaying water protection efficiencies very close to 100%. After the graffiti cleaning cycles, all samples displayed continued low water absorption, showing that the produced coatings were very robust, as the semi-mechanical high pressure cleaning of the stone surface did not affect the coatings' water-repellent functionality significantly, with the Md-W sample displaying the highest water absorption after four cleaning cycles (water protection efficiency of 93±5% after the graffiti cleaning cycles).

Table 8. Static contact angles as received, after coating and after the cleaning cycles.

Sample	**Spray-coated samples**	
	As received	After 4 graffiti cleaning cycles
Pure marble	60±4	62±5
	After coating	After 4 graffiti cleaning cycles
M_d-W	90±4	80±3
M_d-25EG	103±3	78.6±0.5
M_d-25Et	87±2	77±3
M_d-50EG	102±2	76±2
M_d-50Et	86±2	86±2
M_d-100EG	104±3	82±2

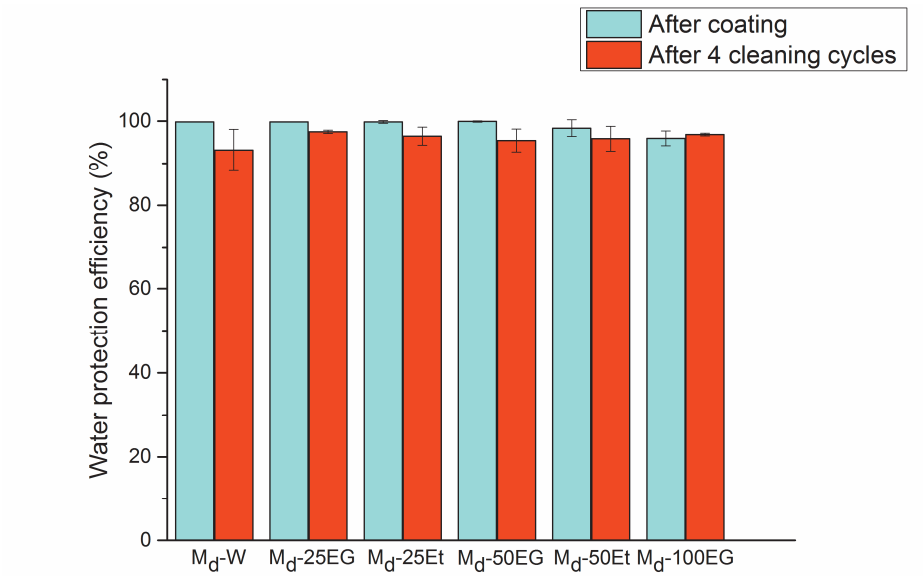

Figure 29. Water protection efficiency of spray-coated stones after functionalization and after four graffiti cleaning cycles.

6.2.2. Determining the effective functionalization depth

In sections 6.1.2.2 and 6.1.2.3, the impact of different co-solvents had on Capstone FS-63 surfactant vesicle behavior was elucidated and it was shown how it was linked to the penetration efficiency into marble stone. While that study focused on the functionalization process in a static system, here the dynamic effects such as the evaporation of the solvent mixture need to be considered (see section 6.2.3 for further details). To investigate the penetration efficiencies of the investigated treatments, a comparison was performed between the samples Md-W, Md-50EG and Md-50Et. The 50% co-solvent coating solutions were selected as they would give the largest difference in performance based on the impact that the co-solvents have on vesicle behavior and penetration depth, as seen in section 6.1.2.3. Thus, these samples were characterized by capillary absorption after UV irradiation and mechanical grinding and the results are presented in Figure 30 and Table 9.

In section 6.1, it was demonstrated that marble samples functionalized by FS-63 using a total immersion method resulted in water absorption as low as 0% even at a depth of 2 mm below the functionalized surface. It was clarified that the solvent polarity was the most important parameter for enhancing the penetration depth, as less polar solvents were able to destabilize the surfactant vesicles. In the functionalization penetration study of these dynamic systems (Figure 30), the samples prepared using the Md-50EG solution performed better than the Md-W

and Md-50Et samples, at least after the intentional UV degradation, suggesting that the EG-based coating method allow the fluorosurfactant to more easily diffuse and react within the marble pores. After grinding 0.5 mm there were no statistically significant differences between the different formulations (analyzed through ANOVA with post-hoc Tukey HSD), although all samples still displayed decreased water absorption compared to similarly ground pure marble, showing that the pore-lining coating was effective at this depth for all the coatings.

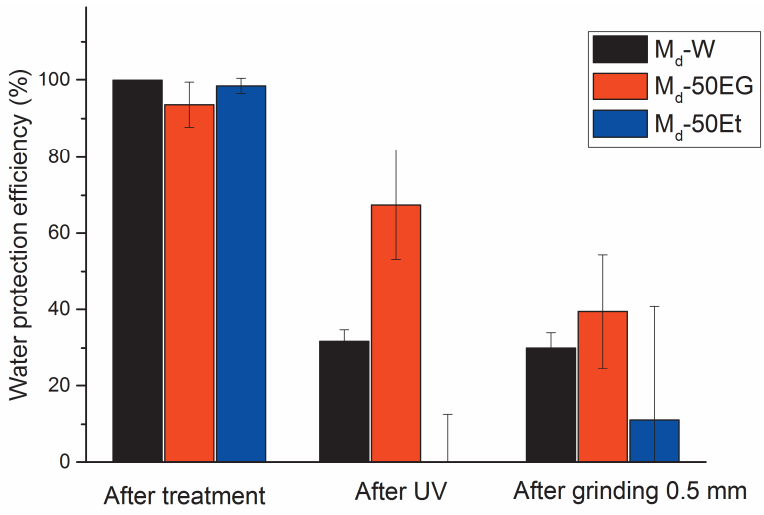

Figure 30. Water protection efficiency of the coatings after treatment, after UV irradiation and after removing 0.5 mm of the outermost surface through sandpaper grinding.

Table 9. Recorded water protection efficiencies after 48 hours.

Solvent used	After treatment	After UV	After 0.5 mm grinding
Md-W	99.8±0%	32±3%	30±4%
Md-50EG	94±6%	70±10%	40±10%
Md-50Et	98±2%	0±10%	10±30%

DLS measurements on the solutions used to coat the stones indicated that the presence of free surfactants or smaller vesicles promotes the penetration of the pore-lining coating even when spray-coated at room temperature. Another contribution to the improved performance for the EG-containing solutions could be related to the slower evaporation rates, which is discussed in greater detail in the following section.

6.2.3. Mechanistic studies on the effect of evaporation kinetics

The evaporation behavior of the coating solutions used for functionalizations in the Md series is presented in Figure 31. From the initial slopes, it is clear that the EtOH-containing solutions evaporate faster than the pure water solution. The point where 10 wt-% of the original solution remains occurred at 5, 2.5 and 2.25 h for the Md-W, Md-25Et and Md-50Et solutions, respectively. As ethanol evaporates concurrently with water, it is difficult to predict the exact compositional changes in those solutions.

The solutions containing ethylene glycol, on the other hand, display a clear two-step evaporation behavior, where the initial slope corresponds well with what is expected from the loss of water. The slower evaporation rates observed for the EG solutions after the departure of water demonstrate why EG-based coatings are beneficial for spray coating, as it would take several days for ethylene glycol-based solutions to evaporate from a coated stone at room temperature. This gives the Capstone FS-63 molecules a longer time to react and diffuse into the pores, which is a clear benefit for coatings intended for outdoor use. The peculiar initial increase in mass for the EG sample can be explained by the hygroscopic nature of ethylene glycol [44], which also can contribute to the slow evaporation rate of the solution.

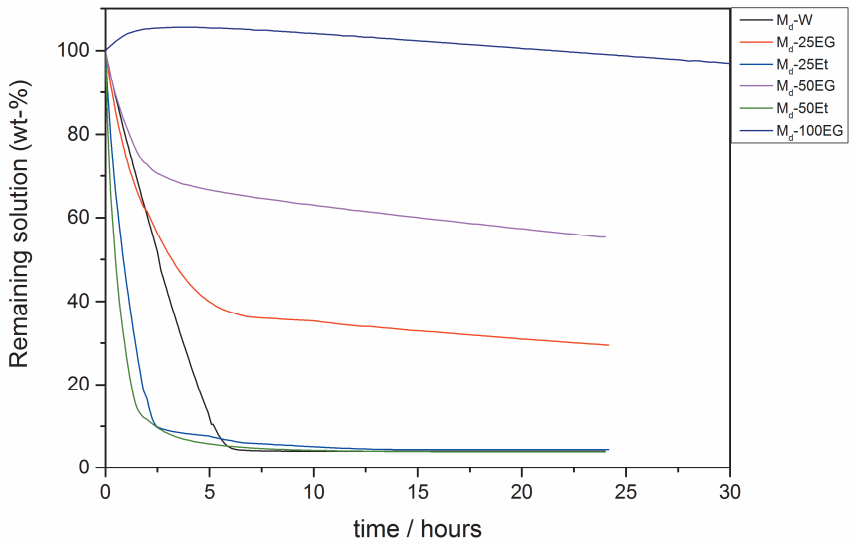

Figure 31. Evaporation kinetics of different solution droplets placed on small marble stones at room temperature, when considering the mass-% solution of the different solutions remaining as a function of time.

As the investigated Md-25EG and Md-50EG solutions contained 10 vol-% Capstone FS-63, which in turn consists of 35% surfactant and 65% volatiles (water and iso-propanol), the mass losses presented in Figure 31 could be used to calculate the theoretical composition of the solutions at different time points. A few assumptions were made in the calculations. Firstly, that no EG evaporated during the 24 h evaporation experiment, and secondly, that the solvent in the pure Capstone FS-63 solution (water and isopropanol, an azeotrope with a boiling point of 80 °C) evaporated ideally with the same rate as water. The estimated composition diagram based on the evaporation kinetics of the Md-25EG and Md-50EG samples showing the compositions in mass-% at different time points is presented in Figure 32a. DLS analysis was performed for solutions corresponding to the estimated solution composition at different times, after the start of the evaporation system (Table 10). The evolution of the micellar aggregates shows that the preferential evaporation of water from the system leads to a decrease in both the z-average size and the vesicle size distribution and concentration of vesicles (Figure 32b&c and Table 10). This is expected as the initial large multilamellar vesicles would shift into small unilamellar and bilamellar vesicles along with the complete destabilization of the vesicles, which increase the amount of free surfactants in the solution [72] upon the evaporation of the volatile phase. This effect is most likely a result of the gradual decrease of the solvent polarity (as the EG concentration increases), which destabilizes the Capstone FS-63 vesicles, releasing free surfactants into the solution. Consequently, this also promotes the diffusion of surfactant molecules into the porous marble. It should be noted that also the viscosity of the system increases upon the preferential evaporation of water, which theoretically could slow down the surfactant diffusion. However, from the grinding results in Figure 30 and Table 9, it is evident that the positive effects that the small vesicle sizes have on the pore functionalization is more important than the negative influence that the high viscosities would give.

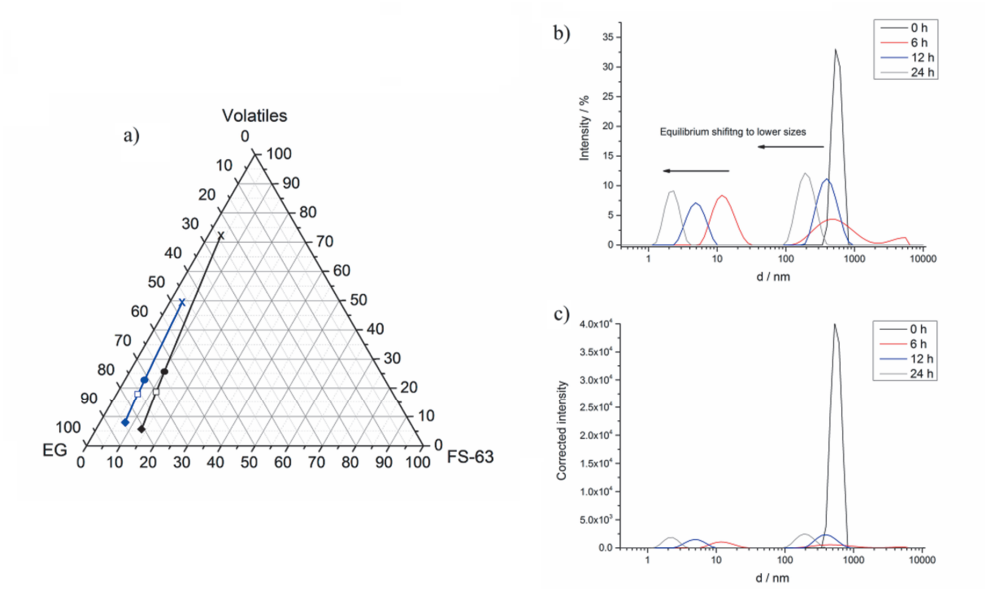

Figure 32. a) Estimated composition diagram based on the evaporation kinetics of the M_d-25EG (black line) and M_d-50EG (blue line) samples showing the compositions in mass-%. The symbols indicate the time points in the evaporation process. Estimated compositions at different times after the start of the experiment is indicated as: X 0 hours, ● 6 hours, □ 12 hours, ◆ 24 hours. b) Particle (or vesicle) size distributions by intensity recorded with DLS as obtained when measured for the M_d-25EG solution c) Particle size distributions recorded with DLS for the M_d-25EG solution, corrected for the vesicle concentrations in the solutions.

Table 10. z-averages determined from DLS measurements.

25-EG					
Time	% Evaporated	Mass Ratio			Z-average [nm]
		FS-63	Volatiles	EG	
0 h	0%	1	19.4	6.5	555±6 nm
6 h	62.5%	1	2.6	6.5	31±3 nm
12 h	68.1%	1	1.7	6.5	21±4 nm
24 h	70.5%	1	0.5	6.5	8.4±0.5 nm

50-EG					
Time	% Evaporated	Mass Ratio			Z-average [nm]
		FS-63	Volatiles	EG	
0 h	0%	1	13.5	13	95±5 nm
6 h	34.2%	1	4.1	13	18±4 nm
12 h	38.3%	1	3	13	11.7±0.2 nm
24 h	44.6%	1	1.3	13	37±3 nm

6.2.3. Anti-graffiti applications of the spray-coated fluorosurfactant functionalization

The graffiti cleanability of the coatings in the M_d series was largely similar with no clear trends, indicating that no formulation was better than the other. The results from these studies are summarized in Figure 33 and Table 11, where the results for the M_d-W coating are shown.

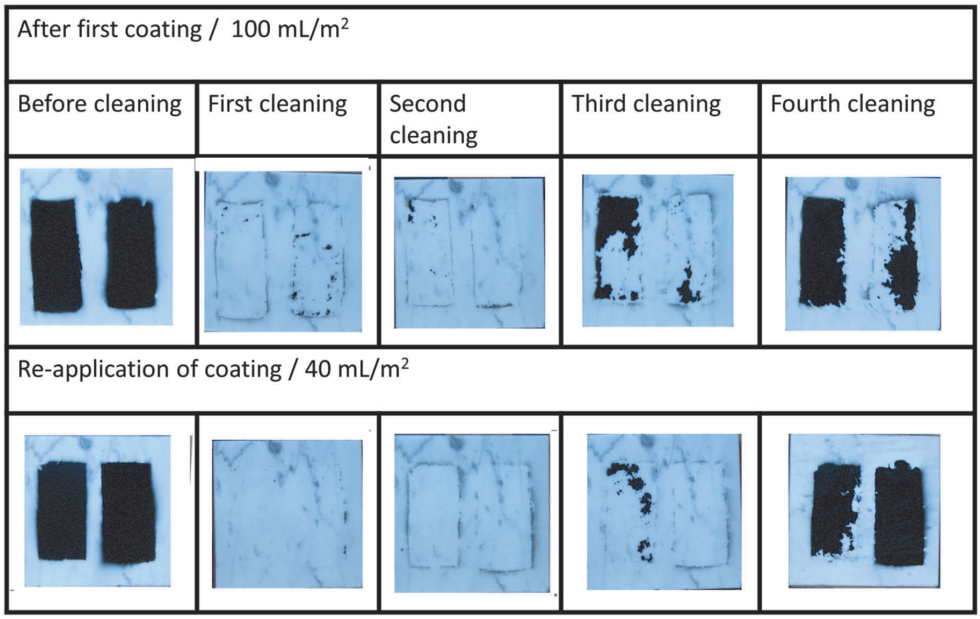

Figure 33. Marble stone (M_d-W) after graffiti cleaning cycles.

Table 11. Percentage Color left on stone after cleaning.

Cleaning	After first coating		After re-application	
	Montana Black	Montana White	Montana Black	Montana White
1st	0.3%	2.3%	0.2%	0.04%
2nd	1.5%	0.2%	0.2%	0.1%
3rd	46.5%	7.0%	16.3%	1.1%
4th	94.8%	40.7%	88.8%	90.6%

There were no large differences in cleanability after the three first graffiti application/cleaning cycles and the graffiti colors were easily removed with a pressure washer. It should be highlighted that untreated marble stones painted with the same graffiti spray paint could not be removed with the pressure washer at all. After the fourth application/cleaning cycle, the excellent cleanability effect was lost.

While the results for the cleaning of Montana White are largely similar to the Montana Black matrix, the nitrocellulose-based Montana Black was slightly harder to wash away. A reason for this could be that nitrocellulose is usually used to modify alkyd resins as to increase the adhesion and hardness of paint films, which also seems to be the case here [102]. The results still demonstrate that the developed fluorosurfactant coating is very robust against both the alkyd resin-based Montana White graffiti paint and the nitrocellulose-based Montana Black paint. It should be noted that after the four graffiti application/cleaning cycles, the stones could be completely cleaned via chemical cleaning, using acetone.

In order to demonstrate the usability of the sprayable Capstone FS-63 solutions as anti-graffiti coatings, new coatings were applied to the samples that had undergone the four initial cleaning cycles. Initially these coatings displayed better cleanability than the same samples after the first coating. This is related to the considerable pore penetration of the surfactant molecules in the first functionalization step (see Section 6.2.2), which in the second step would prevent more surfactants from penetrating into the marble pores, due to the hydrophobized pore openings. This would result in a more tightly packed surface coating of fluorosurfactants on the marble providing the anti-graffiti properties. In the second anti-graffiti testing round, the coatings were also functional for 3 graffiti paint application/cleaning cycles. This indicates that the anti-graffiti effect for the Capstone FS-63 system can be considered semi-permanent as a periodic re-application of the coating is needed when multiple cleaning cycles are to be performed. It has been reported that a successful functionalization of the porous network of a material impacts the anti-graffiti properties positively, as the low surface energy of the pores hinders graffiti absorption [103]. This is one of the causes for the excellent functionality displayed by the pore-penetrating functionalization presented here, as when the second coating is applied, the pores are already functionalized thus providing this benefit.

6.3. Granite protection

6.3.1. Initial characterization of the coatings and stones

The PDMS and Faceal Oleo HD solutions were used to coat the granite samples according to the protocols described in the Materials and methods section. The capillary absorption data after coating is presented in Figure 34 and summarized in Table 12 together with the corresponding contact angles, color differences and water vapor permeability rates.

Table 12. Water contact angles, capillary absorptions, color differences and water vapor permeability rates for the granite stones before and after coating with the different formulations.

Sample	WCA [°]	Capillary absorption [%]	Color difference ΔE^*_{ab}	Q/t [mg/cm²h]
Pure granite	41±3	0±10	-	0.0553±0.0007
G-FO-400	122±2	60±10	0.34	0.0560±0.0003
G-PDMS-20	121±2	70±10	0.83	0.0512±0.0004
G-PDMS-40	124±4	88±6	2.52	-*
G-PDMS-60	120±1	89±6	3.11	0.0513±0.0005
G-PDMS-80	121±3	94±3	3.91	-*
G-PDMS-100	125±1	90±6	5.32	0.0531±0.0005

* Not determined.

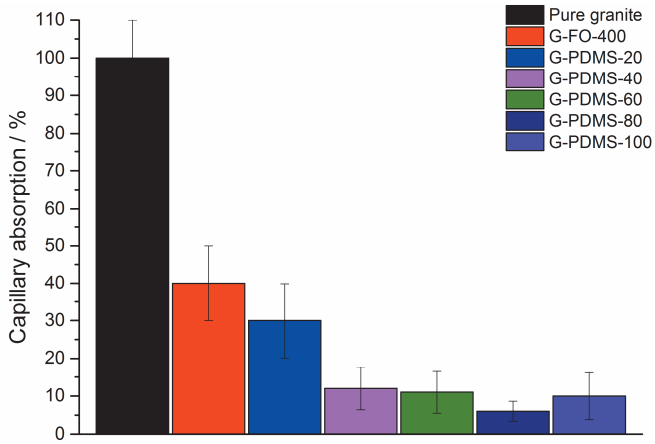

Figure 34. Water protection efficiencies before weathering with the different formulations.

The contact angle measurements showed that the mean water contact angle on the untreated granite stones was 41±3°, while all PDMS coatings gave rise to water contact angles of ~120° or higher, which indicated a successful hydrophobization of the granite surface. Also the Faceal Oleo HD-coated granite stones displayed a contact angle of 122±2°, indicating a successful hydrophobization. The relatively large contact angles were probably a result of the low polarity of the coating material combined with structural effects of the underlying granite surface.

The capillary absorption and standard deviation for nine untreated granite stones were measured to be 0.059±0.008 kg/m² after 48 h on the absorbent bed. The

coated (and weathered) samples were all standardized against this mean value (0.059 kg/m²) according to (7) and the standardized values obtained are presented here. The percentage absorption format was chosen, since it highlights the impact that the weathering effects had on the porosity of granite stones more clearly.

The capillary absorption measurements in Figure 34 showed that the reference coating, Faceal Oleo HD, absorbed 40±10% water compared to pure granite after coating, while the PDMS coated granite stones displayed a decreasing water uptake trend (from 30% to less than 10% compared to pure granite) when the surface coverage was increased from 20 to 100 mL/m². These preliminary results indicated that a PDMS surface coverage of 40 mL/m² or more should be used to block 90% of the water absorption.

The vapor permeability measurements revealed that the coatings did not affect the vapor permeability of the pure granite significantly, as the PDMS-coated granite samples displayed a permeability of about 95% compared to pure granite. The water vapor penetration through a 1 cm thick pure PDMS elastomer layer was found to be negligible, which further proves that the pores were not entirely blocked by PDMS for the coated stones. The Faceal Oleo HD-coated stones displayed a permeability that is within the error margins of the pure granite, which is also what the manufacturer advertises.

In order to investigate if any undesired color alterations occurred to the stone surface, colorimetric measurements were conducted on stones treated with different surface coverage of PDMS, as well as the reference coating of Faceal Oleo HD. All hydrophobized samples were compared to the untreated stones and the color differences are summarized in Table 12. The small measured color changes for the PDMS coatings (ΔE^*_{ab} of about 0.8–5) revealed that no significant discoloring of the granite surface had occurred even when using a PDMS surface coverage of 100 mL/m². It should be noted that the detected differences are slightly above the just noticeable difference level, i.e. $\Delta E^*_{ab} > 2.3$. By reviewing the color difference, it was revealed that the lightness parameter (L) decreased with increasing PDMS coverage, probably as the light reflection decreased slightly with increasing scattering due to the morphological effects from the coatings.

6.3.2. Impact of weathering effects on the coatings and granite stones

The weathering tests showed that the coating stability and the hydrophobic functionality were found to be closely interlinked. As a sufficiently efficient coating could block water from entering the pores, the degradation effects related to salts and water were smaller and the coating was less likely to further degrade

from weathering effects related to water. The benefit of a good protective coating can be seen in Figure 35, where the capillary absorption of the PDMS coatings with a surface coverage above 60 mL/m² displayed unchanged capillary absorption after the different weathering tests, showing the superior stability of this coating. The data for the granite coatings before and after weathering is summarized in Table 13 together with the corresponding contact angles, color differences and mass losses.

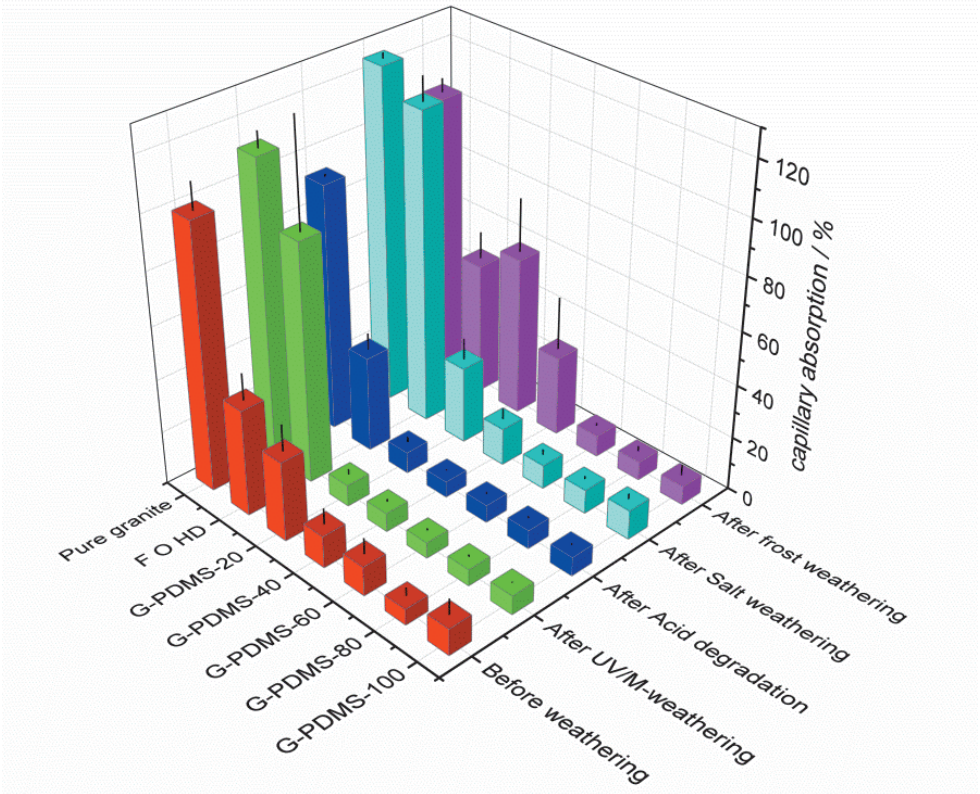

Figure 35. Capillary absorption matrix, showing the capillary water absorption after coating and after the different weathering tests for the investigated coatings.

Table 13. Summarized capillary absorptions, contact angles, color differences and mass losses before and after the weathering tests.

Sample	Before weathering	After UV/M weathering	After acid degradation	After salt weathering	After frost weathering
Capillary absorption [%]					
Pure granite	100±10	112±6	93±1	126±2	106±5
G-FO-400	40±10	90±40	36±6	117±9	50±10
G-PDMS-20	30±10	8±2	8±2	29±8	60±20
G-PDMS-40	12±6	7±1	6.0±0.5	14±4	30±20
G-PDMS-60	11±6	5.9±0.8	6.6±0.8	9±2	8±1
G-PDMS-80	6±3	6.2±0.8	7±1	9±1	7±2
G-PDMS-100	10±6	7.1±0.3	7.1±0.6	11±2	7±4
Water contact angle [°]					
Pure granite	41±3	39±1	44.4±0.6	62±5	60±2
G-FO-400	122±2	5±1	123±1	76±7	106±2
G-PDMS-20	121±2	115±5	119±3	127±7	112±4
G-PDMS-40	124±4	120.5±0.8	116±2	123±3	109±4
G-PDMS-60	120±1	126±2	118±1	131±4	110±10
G-PDMS-80	121±3	121±1	120±3	127±3	109±4
G-PDMS-100	125±1	120±3	116±2	130±6	110±5
Color difference ΔE^*_{ab}					
Pure granite	-	3.32	1.55	1.47	4.6
G-FO-400	0.34	1.73	1.8	2.21	4.77
G-PDMS-20	0.83	1.32	1.18	1.56	2.68
G-PDMS-40	2.52	1.34	4.68	2.71	2.76
G-PDMS-60	3.11	0.34	5.04	4.18	1.4
G-PDMS-80	3.91	0.74	4.25	2.49	3.92
G-PDMS-100	5.32	2.67	4.78	3.8	1.24
Mass loss [%]					
Pure granite	-	0.025±0.001	0.044±0.002	0.5±0.1	0.001±0.001
G-FO-400	-	0.060±0.001	0.055±0.003	0.6±0.1	0.013±0.002
G-PDMS-20	-	0.0221±0.0006	0.040±0.003	0.06±0.01	0.023±0.007
G-PDMS-40	-	0.024±0.003	0.0361±0.0004	0.08±0.08	0.0164±0.003
G-PDMS-60	-	0.0209±0.0004	0.037±0.001	0.07±0.02	0.0180±0.003
G-PDMS-80	-	0.023±0.002	0.0315±0.0006	0.04±0.01	0.0178±0.002
G-PDMS-100	-	0.0215±0.0008	0.0325±0.0009	0.04±0.004	0.0215±0.007

From the UV/M weathering tests, it was evident that UV light is unable to degrade the PDMS network. The reason for this is that PDMS is a very chemically stable hybrid material with a robust silicone backbone that radicals produced by UV radiation simply cannot degrade. The Faceal Oleo HD coating, on the other hand, was completely degraded by UV exposure, as the contact angle decreased from 122±2° (hydrophobic) to 5±1° (hydrophilic), which is significantly lower than the contact angle of pure granite. This degradation was due to radical attack on the less stable acrylic polymer network it consisted of [63]. This change in material properties was also reflected in the large increase in water absorption, from the 36±6% absorption recorded after coating to the significantly higher 90±40% after UV/M weathering.

The effect of acid dissolution on granite can be deduced from the mass losses recorded after the experiment. The pure granite decreased by 0.044±0.002% in mass, while the Faceal Oleo HD-coated sample decreased slightly more, by 0.055±0.003%, and the best PDMS sample decreased by only 0.0315±0.0006%. The positive effect of the PDMS coating is evident in its ability to minimize contact between between the acid and the pure stone surface. While only the front side of the stone is fully protected with the coating (accounting for ~36% of the stone's surface area), 64% of the stone surface area of the PDMS-coated stone is still susceptible to unhindered acid reactions, which accounts for the mass loss these stones displayed.

The damaging effects of salt weathering seem to be the most severe aging mechanism investigated, as seen in Figure 36 and Table 13. The recorded mass losses during this experiment were greater than in any of the other weathering experiments. The mass of the pure granite stones decreased by 0.5±0.1% after 30 salt crystallization cycles, while the Faceal Oleo HD-coated stones displayed a similar mass loss (0.6±0.1%). The PDMS-coated stones, in contrast, displayed mass losses on an order of magnitude lower than the pure granite and Faceal Oleo HD-coated stones (in the range of 0.04–0.08%), which is due to the limited capillary absorption of the coatings that consequently reduces the salt ion diffusion into the pores in these systems.

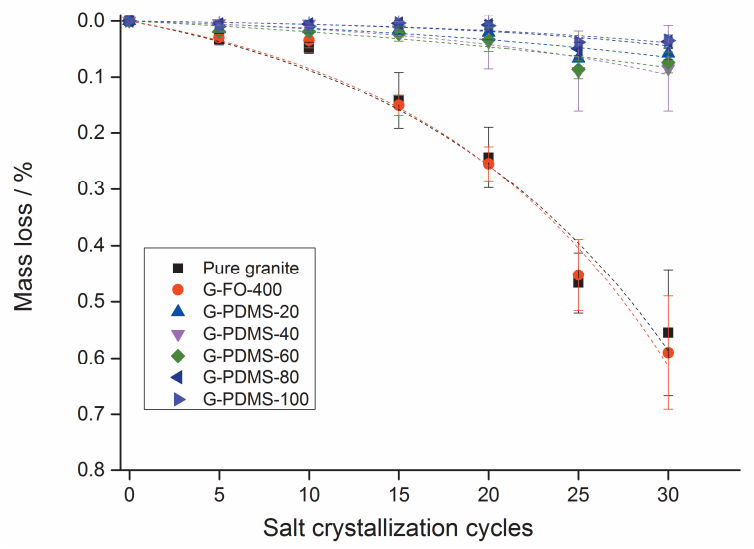

Figure 36. Mass loss of pure and coated granite stones as a function of the number of salt crystallization cycles. The dashed lines are Box Lucas exponential fits, using the model: $y = a(1 - e^{-bx})$, with a Levenberg Marquardt iteration algorithm, which are included as guidelines for data interpretation.

The effect of the salt crystallization cycles was also detectable in the capillary absorption measurements, where the absorption for the pure granite increased by 26 percent units due to the damaging effects of salt crystallization, which increased the open porosity of the granite stones. A similar effect could be seen for the Faceal Oleo HD-coated stones, where the capillary absorption increased from 40±10% after coating to 117±9% after salt weathering, showing that the Faceal Oleo HD coating was ineffective when it comes to preventing salt weathering. The contact angles of the Faceal Oleo HD-coated granite stones had also decreased from 122±2° to 76±7°, demonstrating a detrimental effect of salt weathering on the surface coating. The PDMS-coated granite stones, on the other hand, displayed no large changes in capillary absorption or contact angles after the salt weathering.

Interestingly, the frost weathering appeared to be more detrimental for the protective coating materials than for the granite stone itself. As seen from Table 13, the mass losses recorded for the PDMS- and the Faceal Oleo HD-coated stones after the frost weathering were actually larger than the mass loss recorded for the pure granite. Furthermore, the contact angle for the pristine granite sample was slightly higher after frost weathering, while the percentage of capillary absorption was within the error margins of the unaged sample. The PDMS- and Faceal Oleo HD-coated granite samples displayed a small decrease in contact angles after the 30 freeze-thaw cycles as well as slight deviations in the capillary absorption results, indicating that the coatings were only slightly affected by frost weathering, when capillary absorption and surface hydrophobicity are concerned. Finally, while the recorded color differences were noticeable after freeze-thaw aging, it should be highlighted that the small size of the samples used in this test[9] could have an influence on the results due to the phaneritic nature of granite. The measured color differences are included to show that no large changes occurred from the weathering process.

An interesting observation can be made from the two mechanical weathering tests (i.e. salt and frost weathering) on the pure granite and stones coated with Faceal Oleo HD, where 30 salt crystallization cycles seem to have a much larger impact on the tested stones than 30 freeze-thaw cycles. When considering these weathering effects, it is important to note that freezing water crystallizes into an open hexagonal lattice structure [104], while the sodium sulfate crystallization proceeds via mirabilite crystal growth [105]. Another difference between the frost

[9] Stones with the area of 2x2 cm^2 were used instead of 5x5 cm^2 (as used in the other weathering tests), due to the size restrictions of the container used in the freeze-thaw experiment

and salt weathering is that the freeze-thaw process occurs through frost wedging, i.e. it slowly expands the pores, while salt weathering occurs as a result of internal pressure being applied in the entire salt-filled pore system due to crystal growth. This distinction reveals that frost weathering is more localized, creating far less stress points than in salt weathering, where the effects can be said to be global.

Finally, an important factor to contemplate when considering the overall impact of weathering, is that none of these processes would occur independently in nature. Rather a combination of different weathering effects can augment the weathering impact on pure granite or coated stones. For instance, sunlight may degrade a protective treatment, such as the Faceal Oleo HD coating investigated here, and leave it open to enhanced salt weathering due to increased water and salt absorption.

7. Conclusions

In this study, protective surface functionalizations for marble and granite have successfully been produced and evaluated using new methods.

In the functionalization of marble, the parameters affecting the functionalization efficiency were initially studied under ideal conditions, using a total immersion functionalization method. Initially, the effects of surfactant concentration and reaction time were evaluated to determine the reaction kinetics of the functionalization process and it was found that longer reaction times and higher concentrations were beneficial for functionalization effectiveness. Then the effect of co-solvent composition and temperature during functionalization was studied. Higher reaction temperatures proved to be beneficial for the modification process, while the use of co-solvents, which are less polar than water, proved to affect the surfactant vesicle equilibrium, shifting the equilibrium towards free surfactants and consequently improving the molecular dynamics of the system and giving better pore modifications compared to other systems.

The marble functionalization system, optimized under ideal reaction conditions, was then adapted to a dynamic application scheme, utilizing spray coating for marble pore penetration and functionalization with fluorosurfactants under room temperature conditions. Also in this system, the effect of different co-solvents was studied and it was found that the addition of ethylene glycol gave the best results, when a successful pore penetration was the goal. As the slow evaporation rate of ethylene glycol enabled a longer reaction time for the fluorosurfactants, the best results were obtained when using EG-rich spray coating solutions.

The applicability and stability of a PDMS coating for granite was also studied with the focus on different weathering effects using simulated weathering methods. It was found that with a sufficient surface coverage, all the studied weathering effects could be prevented. The ability of the coating to inhibit water uptake hindered salt from being introduced into the pores and by this means salt weathering could be minimized.

8. Further studies

Further studies in this field could focus on the use of surfactants in different coating applications using the methods developed in this thesis. Controlling simple parameters such as solution temperature and co-solvent composition could potentially improve the coating efficacy of surfactants used in coating production of different porous materials.

The superb stability demonstrated for the PDMS coatings could also be applied for the protection of other substrates than granite, providing a long term protection for a variety of surfaces. This would be very beneficial for the marine and automotive industries.

Regarding the studies conducted here, the marble functionalizations (Papers **I**-**III**) could be evaluated by a proper weathering durability test, such as the one presented in Paper **IV**. Another subject that could be of interest, as the coatings can be easily applied by spray coating, is the scale-up of the presented spray coating method, which will be very useful for hydrophobizing large stone objects and for the retrofitting of buildings and bridges.

If the protection of important historical marble monuments are considered with the fluorosurfactant total immersion method, further studies should be carried out on the effects the immersion and higher temperatures the functionalizations have on marble from a (poro)mechanical standpoint.

8. Acknowledgements

The author wishes to express his sincere thanks to Docent Jan-Henrik Smått and Professor Jouko Peltonen for their inspiring guidance and never failing enthusiastic support throughout the work underlying this thesis.

During this work the author has had a very pleasant and stimulating cooperation with Dr. Andreas Bergbreiter, Professor Mika Lindén, Mr. Petteri Kinnunen, M.Sc., Mr. Richard Fogde, M.Sc., Professor David Grosso, Dr. Monika Kümmel, Dr. Benjamin Louis, Dr. Leif kronberg and Mr. Axel Meijerjohann, M.Sc.

I also want to thank all my colleagues at the Laboratory of Physical Chemistry, Åbo Akademi University, for enjoyable cooperation and fellowship.

Furthermore, I wish to express my sincere thanks to Mr. Kenneth Stenlund, M.Sc., for his help designing the experimental equipment and his fellowship and Mrs. Christina Luojola, M.Sc., is thanked for helping with all the administrative work related to work in science these days.

The author wishes to express his sincere thanks to Coligro Oy (2010-2014), Tekes (2010-2014), Magnus Ehrnrooths stiftelse (2015), Svenska Kulturfonden (2015-2016) and K.H. Renlunds Stiftelse (2015-2016) for the financial support provided.

Last but not least, I wholeheartedly appreciate the tireless support my family and friends has given me since day one. Thank you all!

9. References

[1] D. Camuffo, Physical weathering of stones, Sci Total Environ. 167 (1995) 1-14.

[2] M. Sadat-Shojai, A. Ershad-Langroudi, Polymeric coatings for protection of historic monuments: Opportunities and challenges, J Appl Polym Sci. 112 (2009) 2535-2551.

[3] G. Giuntoli, L. Rosi, M. Frediani, B. Sacchi, P. Frediani, Fluoro-functionalized PLA polymers as potential water-repellent coating materials for protection of stone, J Appl Polym Sci. 125 (2012) 3125-3133.

[4] M. Licchelli, S.J. Marzolla, A. Poggi, C. Zanchi, Crosslinked fluorinated polyurethanes for the protection of stone surfaces from graffiti, J Cult Herit. 12 (2011) 34-43.

[5] L. Toniolo, T. Poli, V. Castelvetro, A. Manariti, O. Chiantore, M. Lazzari, Tailoring new fluorinated acrylic copolymers as protective coatings for marble, J Cult Herit. 3 (2002) 309-316.

[6] C.D. Vacchiano, L. Incarnato, P. Scarfato, D. Acierno, Conservation of tuff-stone with polymeric resins, Constr Build Mater. 22 (2008) 855-865.

[7] O. Chiantore, M. Lazzari, Photo-oxidative stability of paraloid acrylic protective polymers, Polymer. 42 (2001) 17-27.

[8] M. Favaro, R. Mendichi, F. Ossola, U. Russo, S. Simon, P. Tomasin, P.A. Vigato, Evaluation of polymers for conservation treatments of outdoor exposed stone monuments. Part I: Photo-oxidative weathering, Polym Degrad Stab. 91 (2006) 3083-3096.

[9] A. Tsakalof, P. Manoudis, I. Karapanagiotis, I. Chryssoulakis, C. Panayiotou, Assessment of synthetic polymeric coatings for the protection and preservation of stone monuments, J Cult Herit. 8 (2007) 69-72.

[10] L. de Ferri, P.P. Lottici, A. Lorenzi, A. Montenero, E. Salvioli-Mariani, Study of silica nanoparticles – polysiloxane hydrophobic treatments for stone-based monument protection, J Cult Herit. 12 (2011) 356-363.

[11] E.K. Kim, J. Won, J. Do, S.D. Kim, Y.S. Kang, Effects of silica nanoparticle and GPTMS addition on TEOS-based stone consolidants, J Cult Herit. 10 (2009) 214-221.

[12] P.N. Manoudis, A. Tsakalof, I. Karapanagiotis, I. Zuburtikudis, C. Panayiotou, Fabrication of super-hydrophobic surfaces for enhanced stone protection, Surf Coat Tech. 203 (2009) 1322-1328.

[13] Z. Guo, W. Liu, B. Su, Superhydrophobic surfaces: From natural to biomimetic to functional, J Colloid Interface Sci. 353 (2011) 335-355.

[14] D. Ebert, B. Bhushan, Durable Lotus-effect surfaces with hierarchical structure using micro- and nanosized hydrophobic silica particles, J Colloid Interface Sci. 368 (2012) 584-591.

[15] C. Chiavari, A. Balbo, E. Bernardi, C. Martini, F. Zanotto, I. Vassura, M.C. Bignozzi, C. Monticelli, Organosilane coatings applied on bronze: Influence of UV radiation and thermal cycles on the protectiveness, Prog Org Coat. 82 (2015) 91-100.

[16] F. Xu, C. Wang, D. Li, M. Wang, F. Xu, X. Deng, Preparation of modified epoxy–SiO_2 hybrid materials and their application in the stone protection, Prog Org Coat. 81 (2015) 58-65.

[17] C. Kapridaki, P. Maravelaki-Kalaitzaki, TiO_2–SiO_2–PDMS nano-composite hydrophobic coating with self-cleaning properties for marble protection, Prog Org Coat. 76 (2013) 400-410.

[18] Y. Luo, L. Xiao, X. Zhang, Characterization of TEOS/PDMS/HA nanocomposites for application as consolidant/hydrophobic products on sandstones, J Cult Herit. 16 (2015) 470-478.

[19] D. Li, F. Xu, Z. Liu, J. Zhu, Q. Zhang, L. Shao, The effect of adding PDMS-OH and silica nanoparticles on sol–gel properties and effectiveness in stone protection, Appl Surf Sci. 266 (2013) 368-374.

[20] I. De Rosario, F. Elhaddad, A. Pan, R. Benavides, T. Rivas, M.J. Mosquera, Effectiveness of a novel consolidant on granite: Laboratory and in situ results, Constr Build Mater. 76 (2015) 140-149.

[21] G.C. Borgia, M. Camaiti, F. Cerri, P. Fantazzini, F. Piacenti, Study of water penetration in rock materials by Nuclear Magnetic Resonance Tomography: hydrophobic treatment effects, J Cult Herit. 1 (2000) 127-132.

[22] P. Meloni, F. Manca, G. Carcangiu, Marble protection: An inorganic electrokinetic approach, Appl Surf Sci. 273 (2013) 377-385.

[23] M. Järn, M. Heikkilä, M. Lindén, Bioinspired Synthesis of Superhydrophobic Coatings, Langmuir. 24 (2008) 10625-10628.

[24] W. El Malti, D. Laurencin, G. Guerrero, M.E. Smith, P.H. Mutin, Surface modification of calcium carbonate with phosphonic acids, J Mater Chem. (2012) 1212-1218.

[25] T. Nakatsuka, H. Kawasaki, K. Itadani, S. Yamashita, Topochemical reaction of calcium carbonate and alkyl dihydrogenphosphate, J. Colloid Interface Sci. 82 (1981) 298-306.

[26] J. Kiehl, C. Ben-Azzouz, D. Dentel, M. Derivaz, J.L. Bischoff, C. Delaite, S. Bistac, Grafting process of ethyltrimethoxysilane and polyphosphoric acid on calcium carbonate surface, Appl Surf Sci. 264 (2013) 864-871.

[27] D. Stout, S. Semaw, M.J. Rogers, D. Cauche, Technological variation in the earliest Oldowan from Gona, Afar, Ethiopia, J Hum Evol. 58 (2010) 474-491.

[28] K. Buche, R. Grapes, Petrogenesis of Metamorphic Rocks, 8th ed., Springer-Verlag GmbH, Berlin, Germany, 2011.

[29] C. Klein, C.S.J. Hurlbut, Manual of Mineralogy, 21st ed., John Wiley & sons, inc., USA, 1993.

[30] http://www.davidchipperfield.co.uk/, accessed 22.7.2016.

[31] M.K. Gökay, I.B. Gundogdu, Color identification of some Turkish marbles, Constr Build Mater. 22 (2008) 1342-1349.

[32] A. Šťastná, R. Přikryl, J. Jehlička, Methodology of analytical study for provenance determination of calcitic, calcite–dolomitic and impure marbles from historical quarries in the Czech Republic, J Cult Herit. 10 (2009) 82-93.

[33] J. Ruedrich, D. Kirchner, S. Siegesmund, Physical weathering of building stones induced by freeze–thaw action: a laboratory long-term study, Environ Earth Sci. 63 (2011) 1573--1586.

[34] D.M. Freire-Lista, R. Fort, M.J. Varas-Muriel, Freeze–thaw fracturing in building granites, Cold Reg. Sci Technol. 113 (2015) 40-51.

[35] N. Matsuoka, Frost weathering and rockwall erosion in the southeastern Swiss Alps: Long-term (1994–2006) observations, Geomorphology. 99 (2008) 353-368.

[36] UNESCO-RILEM, Réunion Internationale des Laboratoires d'Essais et de recherche sur les matériaux et les Constructions (RILEM). Crystallization test by total immersion (Test V. 1.) Crystallization test by partial immersion (Test V.2.), Proceed. Intern. Symposium Deterioration and Conservation of Stone monuments. (1978).

[37] S.L. Goldstone, S.C. Francis, S.J. Gardner, An investigation into the enhancement of sea-spray exposed fingerprints on glass, Forensic Sci Int. 252 (2015) 33-38.

[38] E. Rothert, T. Eggers, J. Cassar, J. Ruedrich, B. Fitzner, S. Siegesmund, Stone properties and weathering induced by salt crystallization of Maltese Globigerina Limestone, Geological Society, London, Special Publications. 271 (2007) 189-198.

[39] J.M. Vallet, C. Gosselin, P. Bromblet, O. Rolland, V. Vergès-Belmin, W. Kloppmann, Origin of salts in stone monument degradation using sulphur and oxygen isotopes: First results of the Bourges cathedral (France), J Geochem Explor. 88 (2006) 358-362.

[40] Y. Ocak, A. Sofuoglu, F. Tihminlioglu, H. Böke, Protection of marble surfaces by using biodegradable polymers as coating agent, Prog Org Coat. 66 (2009) 213-220.

[41] E.S. Chardon, F.R. Livens, D.J. Vaughan, Reactions of feldspar surfaces with aqueous solutions, Earth-Sci Rev. 78 (2006) 1-26.

[42] Y. Yang, Y. Min, J. Lococo, Y. Jun, Effects of Al/Si ordering on feldspar dissolution: Part I. Crystallographic control on the stoichiometry of dissolution reaction, Geochim Cosmochim Acta. 126 (2014) 574-594.

[43] Y. Yang, Y. Min, Y. Jun, Effects of Al/Si ordering on feldspar dissolution: Part II. The pH dependence of plagioclases' dissolution rates, Geochim Cosmochim Acta. 126 (2014) 595-613.

[44] P. Sanmartín, F. Cappitelli, R. Mitchell, Current methods of graffiti removal: A review, Constr Build Mater. 71 (2014) 363-374.

[45] P. Sanmartín, A. DeAraujo, A. Vasanthakumar, R. Mitchell, Feasibility study involving the search for natural strains of microorganisms capable of degrading graffiti from heritage materials, Int Biodeterior Biodegrad. 103 (2015) 186-190.

[46] C. Esposito Corcione, R. Striani, M. Frigione, Novel hydrophobic free-solvent UV-cured hybrid organic–inorganic methacrylic-based coatings for porous stones, Prog Org Coat. 77 (2014) 803-812.

[47] L. D'Arienzo, P. Scarfato, L. Incarnato, New polymeric nanocomposites for improving the protective and consolidating efficiency of tuff stone, J Cult Herit. 9 (2008) 253-260.

[48] E. Franzoni, E. Sassoni, G. Graziani, Brushing, poultice or immersion? The role of the application technique on the performance of a novel hydroxyapatite-based consolidating treatment for limestone, J Cult Herit. 16 (2015) 173-184.

[49] M. Licchelli, S.J. Marzolla, A. Poggi, C. Zanchi, Crosslinked fluorinated polyurethanes for the protection of stone surfaces from graffiti, J Cult Herit. 12 (2011) 34-43.

[50] Y. Ocak, A. Sofuoglu, F. Tihminlioglu, H. Böke, Sustainable bio-nano composite coatings for the protection of marble surfaces, J Cult Herit. 16 (2015) 299-306

[51] C. Esposito Corcione, R. Striani, M. Frigione, UV-cured siloxane-modified methacrylic system containing hydroxyapatite as potential protective coating for carbonate stones, Prog Org Coat. 76 (2013) 1236-1242.

[52] J. Kapolos, N. Bakaoukas, A. Koliadima, G. Karaiskakis, Evaluation of acrylic polymeric resin and small siloxane molecule for protecting cultural heritage monuments against sulfur dioxide corrosion, Prog Org Coat. 59 (2007) 152-159.

[53] C. Kapridaki, L. Pinho, M.J. Mosquera, P. Maravelaki-Kalaitzaki, Producing photoactive, transparent and hydrophobic SiO_2-crystalline TiO_2 nanocomposites at ambient conditions with application as self-cleaning coatings, Appl Catal B. 156–157 (2014) 416-427.

[54] I. Karapanagiotis, A. Pavlou, P.N. Manoudis, K.E. Aifantis, Water repellent ORMOSIL films for the protection of stone and other materials, Mater Lett. 131 (2014) 276-279.

[55] H. Zhang, Q. Liu, T. Liu, B. Zhang, The preservation damage of hydrophobic polymer coating materials in conservation of stone relics, Prog Org Coat. 76 (2013) 1127-1134.

[56] R. Ion, D. Turcanu-Caruțiu, R. Fierăscu, I. Fierăscu, I. Bunghez, M. Ion, S. Teodorescu, G. Vasilievici, V. Rădițoiu, Caoxite-hydroxyapatite composition as consolidating material for the chalk stone from Basarabi–Murfatlar churches ensemble, Appl Surf Sci. 358, Part B (2015) 612-618.

[57] M. Ludovico-Marques, C. Chastre, Effect of consolidation treatments on mechanical behaviour of sandstone, Constr Build Mater. 70 (2014) 473-482.

[58] A. Zornoza-Indart, P. Lopez-Arce, Silica nanoparticles (SiO_2): Influence of relative humidity in stone consolidation, J Cult Herit. 18 (2016) 258-270

[59] M. Lettieri, M. Masieri, Surface characterization and effectiveness evaluation of anti-graffiti coatings on highly porous stone materials, Appl Surf Sci. 288 (2014) 466-477.

[60] O. García, K. Malaga, Definition of the procedure to determine the suitability and durability of an anti-graffiti product for application on cultural heritage porous materials, J Cult Herit. 13 (2012) 77-82.

[61] H.H. Teng, A. Puli, M. Karakouzian, X. Xu, Identification of Graffiti Countermeasures for Highway Facilities, Procedia - Soc Behav Sci. 43 (2012) 681-691.

[62] A. Ghasemi-Kahrizsangi, J. Neshati, H. Shariatpanahi, E. Akbarinezhad, Improving the UV degradation resistance of epoxy coatings using modified carbon black nanoparticles, Prog Org Coat. 85 (2015) 199-207.

[63] G. Cappelletti, P. Fermo, M. Camiloni, Smart hybrid coatings for natural stones conservation, Prog Org Coat. 78 (2015) 511-516.

[64] R.M. Pashley, M.E. Karaman, Applied Colloid and Surface Chemistry, 1st ed., Wiley, Chichester, West Sussex, England, Gerat Britain, 2004.

[65] M. Härth, D.W. Schubert, Simple Approach for Spreading Dynamics of Polymeric Fluids, Macromol Chem Phys. 213 (2012) 654-665.

[66] J. Bear, Dynamics of Fluids in Porous Media, Dover ed., Elsevier Publishing Company Inc., New york, U.S.A., 1988.

[67] J. Cai, E. Perfect, C-L. Cheng, X. Hu, Generalized Modeling of Spontaneous Imbibition Based on Hagen–Poiseuille Flow in Tortuous Capillaries with Variably Shaped Apertures, Langmuir. 30 (2014) 5142-5151.

[68] W.F. Pickard, The ascent of sap in plants, Prog. Biophys. Mol. Biol. 37 (1981) 181-229.

[69] J. Israelachvili, D. Mitchell, B. Ninham, Theory of Self-Assembly of Hydrocarbon Amphiphiles into Micelles and Bilayers, J Chem Soc Faraday Trans. 72 (1976) 1525-1568.

[70] S. Consola, M. Blanzat, E. Perez, J. Garrigues, P. Bordat, I. Rico-Lattes, Design of Original Bioactive Formulations Based on Sugar–Surfactant/Non-steroidal Anti-inflammatory Catanionic Self-Assemblies: A New Way of Dermal Drug Delivery, Chem Euro J. 13 (2007) 3039-3047.

[71] J.N. Israelachvili, Intermolecular and Surface Forces, 3rd ed., Academic Press, San Diego, 2011.

[72] J. Drazenovic, H. Wang, K. Roth, J. Zhang, S. Ahmed, Y. Chen, G. Bothun, S.L. Wunder, Effect of lamellarity and size on calorimetric phase transitions in single component phosphatidylcholine vesicles, Biochim Biophys Acta - Biomembranes. 1848 (2015) 532-543.

[73] N. Dharaiya, P. Bahadur, K. Singh, D.G. Marangoni, P. Bahadur, Light scattering and NMR studies of Triton X-100 micelles in the presence of short chain alcohols and ethoxylates, Colloids Surf Physicochem Eng Aspects. 436 (2013) 252-259.

[74] V.I. Martín, A. Rodríguez, A. Laschewsky, M.L. Moyá, Self-aggregation of cationic dimeric surfactants in water–ionic liquid binary mixtures, J Colloid Interface Sci. 430 (2014) 326-336.

[75] J. Dey, S. Kumar, A. Srivastava, G. Verma, P.A. Hassan, V.K. Aswal, J. Kohlbrecher, K. Ismail, Effect of ethylene glycol on the special counterion binding and microstructures of sodium dioctylsulfosuccinate micelles, J Colloid Interface Sci. 414 (2014) 103-109.

[76] J.B. Rosenholm, Phase equilibriums, self-assembly and interactions in two-, three- and four medium-chain length component systems, Adv Colloid Interface Sci. 205 (2014) 9-47.

[77] A. Chaudhuri, S. Haldar, A. Chattopadhyay, Structural transition in micelles: novel insight into microenvironmental changes in polarity and dynamics, Chem Phys Lipids. 165 (2012) 497-504.

[78] C.J.F. Rijcken, O. Soga, W.E. Hennink, C.F. van Nostrum, Triggered destabilisation of polymeric micelles and vesicles by changing polymers polarity: An attractive tool for drug delivery, J Controlled Release. 120 (2007) 131-148.

[79] E.A.M. Al-Sherbini, M.H. Abdel-Kader, R.Y. Hamzah, Effect of binary solvents on the critical micelles concentration by using 1-methyl-4-[4'-aminostyryl]pyridinium iodide, Colloids Surf Physicochem Eng Aspects. 194 (2001) 133-142.

[80] K. Malaga-Starzec, J.E. Lindqvist, B. Schouenborg, Experimental study on the variation in porosity of marble as a function of temperature, in: S. Siegesmund, T. Weiss, A. Vollbrecht (Eds.), Natural Stone, Weathering Phenomena, Conservation Strategies and Case Studies, Geological Society, London. 205 (2002) 81–88.

[81] M.R. Ramli, M.B.H. Othman, A. Arifin, Z. Ahmad, Cross-link network of polydimethylsiloxane via addition and condensation (RTV) mechanisms. Part I: Synthesis and thermal properties, Polym Degrad Stab. 96 (2011) 2064-2070.

[82] EN 15801:2010, Conservation of cultural property test methods, Determination of water absorption by capillarity, European standard (2010).

[83] EN 15886:2010, Conservation of cultural property test methods, Colour measurement of surfaces, European standard (2010).

[84] T. Young, an essay on the cohesion of fluids, Philos Trans R Soc Lond. 95 (1805) 65-87.

[85] T. Song, S. Dai, K.C. Tam, S.Y. Lee, S.H. Goh, Aggregation behavior of two-arm fullerene-containing poly(ethylene oxide), Polymer. 44 (2003) 2529-2536.

[86] V. Bardik, V. Gotsulskii, E. Pavlov, N. Malomuzh, D. Nerukh, I. Yanchuk, S. Lavoryk, Light scattering study of human serum albumin in pre-denaturation: Relation to dynamic transition in water at 42 °C, J Mol Liq. 176 (2012) 60-64.

[87] S.J. Wallace, J. Li, R.L. Nation, B.J. Boyd, Drug release from nanomedicines: Selection of appropriate encapsulation and release methodology, Drug Deliv Transl Res. 2 (2012) 284.

[88] A. Lapresta-Fernández, J.M. García-García, R. París, R. Huertas-Roa, A. Salinas-Castillo, S.A. de la Llana, J.F. Huertas-Pérez, N. Guarrotxena, L.F. Capitán-Vallvey, I. Quijada-Garrido, Thermoresponsive Gold Polymer Nanohybrids with a Tunable Cross-Linked MEO2MA Polymer Shell, Part Part Sys Charact. 31 (2014) 1183-1191.

[89] Q. Liu, S. Chen, J. Chen, J. Du, An Asymmetrical Polymer Vesicle Strategy for Significantly Improving T1 MRI Sensitivity and Cancer-Targeted Drug Delivery, Macromolecules. 48 (2015) 739-749.

[90] P. Sun, D. Zhou, Z. Gan, Novel reduction-sensitive micelles for triggered intracellular drug release, J Controlled Release. 155 (2011) 96-103.

[91] H. Patel, G. Raval, M. Nazari, H. Heerklotz, Effects of glycerol and urea on micellization, membrane partitioning and solubilization by a non-ionic surfactant, Biophys Chem. 150 (2010) 119-128.

[92] A Basic Introduction to Rheology, Bohlin Instruments Ltd, The Corinium Centre, Cirencester, Glos., Great Britain (1994).

[93] Standard Test Method for Evaluation of Durability of Rock for Erosion Control Under Freezing and Thawing Conditions, ASTM standard D 5312-04A (2004).

[94] Exposure procedure for artificial weathering, EOTA technical report. TR 010 (2004).

[95] A. Torrisi, Evaluation of five fluorinated compounds as calcarenite protectives, J Cult Herit. 9 (2008) 135-145.

[96] P. Rizzarelli, C. La Rosa, A. Torrisi, Testing a fluorinated compound as a protective material for calcarenite, J Cult Herit. 2 (2001) 55-62.

[97] V. Di Tullio, N. Proietti, D. Capitani, I. Nicolini, A.M. Mecchi, NMR depth profiles as a non-invasive analytical tool to probe the penetration depth of hydrophobic treatments and inhomogeneities in treated porous stones, Anal Bioanal Chem. 400 (2011) 3151-3164.

[98] D. Van de Walle, P. Goossens, K. Dewettinck, Influence of the polarity of the water phase on the mesomorphic behaviour and the α-gel stability of a commercial distilled monoglyceride, Food Res Int. 41 (2008) 1020-1025.

[99] I.M. Smallwood, Solvent Recovery Handbook, 2nd ed., CRC Press, Boca Raton, USA, 2002.

[100] L. Dumée, J.L. Campbell, K. Sears, J. Schütz, N. Finn, M. Duke, S. Gray, The impact of hydrophobic coating on the performance of carbon nanotube bucky-paper membranes in membrane distillation, Desalination. 283 (2011) 64-67.

[101] L. Dumée, V. Germain, K. Sears, J. Schütz, N. Finn, M. Duke, S. Cerneaux, D. Cornu, S. Gray, Enhanced durability and hydrophobicity of carbon nanotube bucky paper membranes in membrane distillation, J Membr Sci. 376 (2011) 241-246.

[102] G. Germinario, I.D. van der Werf, L. Sabbatini, Chemical characterisation of spray paints by a multi-analytical (Py/GC–MS, FTIR, μ-Raman) approach, Microchem J. 124 (2016) 929-939.

[103] J. Scheerder, N. Visscher, T. Nabuurs, A. Overbeek, Novel, water-based fluorinated polymers with excellent antigraffiti properties, J Coating Tech Res. 2 (2005) 617-625.

[104] M. Akyurt, G. Zaki, B. Habeebullah, Freezing phenomena in ice–water systems, Energ Convers Manage. 43 (2002) 1773-1789.

[105] C. Rodriguez-Navarro, E. Doehne, E. Sebastian, How does sodium sulfate crystallize? Implications for the decay and testing of building materials, Cem Concr Res. 30 (2000) 1527-1534.

ISBN 978-952-12-3498-9